ARCHIWIND

VALIDATION REPORT

Knut Erik T. Giljarhus & Samuele Patelli
NablaFlow
September 2026

ABSTRACT

This report presents validation examples of ArchiWind's standard CFD workflow. Two test cases are presented, one for wind speed in terrain, and one for pedestrian wind assessment in an urban environment. For terrain, the Askervein Hill test case is used, while for urban environments, the AIJ Benchmark Case E (Niigata) is used. Results demonstrate good agreement with field data and wind tunnel data and confirm that ArchiWind accurately captures key phenomena relevant for decision-making processes for construction in terrain and urban environments.

1. ARCHIWIND METHODOLOGY

Archiwind uses OpenFOAM to generate and solve three-dimensional wind-flow models over terrain. The flow is treated as incompressible, neutrally stratified and statistically steady. The simulations are performed using the simpleFoam solver, which solves the steady incompressible Reynolds-averaged Navier-Stokes equations using the SIMPLE pressure-velocity coupling algorithm.

Turbulence is represented using the realizable k-epsilon model. This is a two-equation eddy-viscosity closure in which transport equations are solved for turbulent kinetic energy, (k), and turbulent dissipation rate. The realizable formulation differs from the standard k-epsilon model through a variable model coefficient and a modified dissipation-rate equation intended to improve the representation of flows involving strain, rotation and separation. Numerical schemes are selected to provide a suitable balance between robustness and accuracy.

The atmospheric inlet is specified assuming a homogeneous, dry, equilibrium and neutrally stratified atmospheric boundary layer using a logarithmic mean-velocity profile.

The terrain is treated using an aerodynamic rough-wall condition consistent with the roughness length used in the atmospheric inlet. This consistency is important because a mismatch between inlet and ground boundary conditions can cause the atmospheric profile to accelerate or decelerate as it develops through the domain.

The computational mesh is an unstructured, hex-dominated mesh, generated automatically based on best practice guidelines and the given surface geometries. The details of the mesh for each validation case is given in each separate section.

2. FLOW OVER TERRAIN

The validation presented in this section is intended to assess the suitability of the Archiwind methodology for predicting mean wind speed over terrain. The principal validation quantity is the terrain-induced speed-up at specified heights above the local ground, relevant for determining load factors for local construction.

2.1 THE ASKERVEIN HILL

The Askervein Hill experiment was selected because it is one of the most extensively documented full-scale field experiments of atmospheric flow over an isolated hill. The experiments were conducted in 1982 and 1983 at Askervein on South Uist in the Outer Hebrides of Scotland [8]. The hill is approximately 116 m high, and more than 50 instrumented towers were deployed during the campaigns. Measurements were obtained along several lines crossing the hill and at an upstream reference location.

The Askervein case is particularly suitable for the present purpose because it combines full-scale atmospheric-boundary-layer conditions with relatively simple terrain and extensive measurements of

mean velocity. The commonly studied TU03-B run represents approximately neutral atmospheric conditions with wind approaching from the southwest, where the upstream terrain is relatively flat and uniform. This permits the effects of the hill to be distinguished from major upstream terrain disturbances.

2.1.1 CASE DESCRIPTION AND CFD SETUP

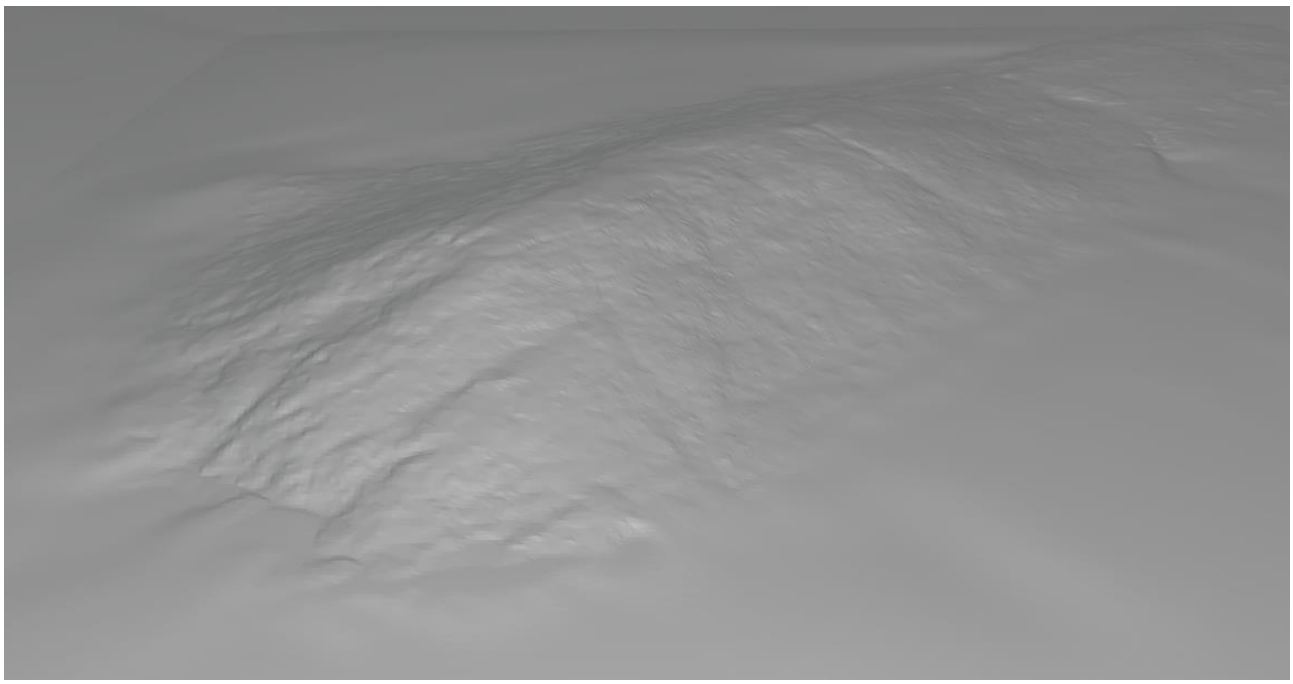


FIGURE 1 – 3D ORTHOGRAPHIC VIEW OF THE ASKERVEIN HILL.

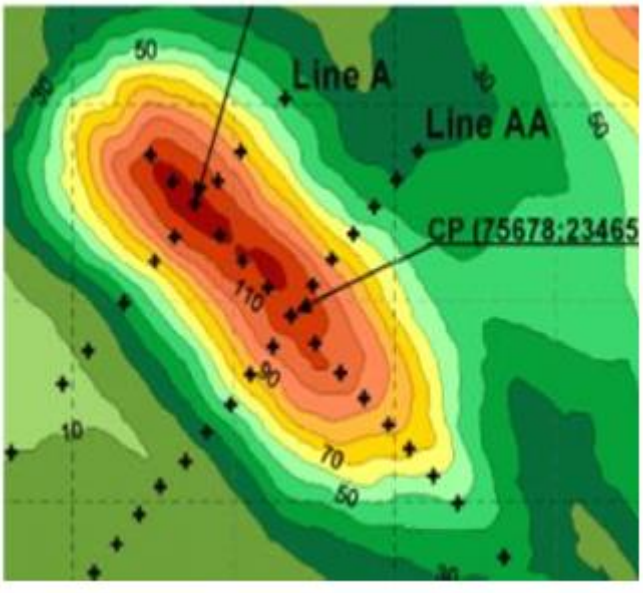


FIGURE 2 – LOCATION OF MEASUREMENT POINTS.

The simulated geometry is shown in Figure 1. The terrain geometry was generated from the available Askervein digital topography, with a resolution of 5m. The surrounding downstream of the hill was removed from the model, consistent with other benchmark simulations of this case.

The validation is based on the TU03-B experimental run. This run is widely used because the atmospheric conditions were approximately neutral and the wind approached from the relatively unobstructed southwest sector.

The terrain roughness is treated as spatially uniform with z0=0.03 m for the primary validation calculation. This value represents the low vegetation and rough open terrain surrounding Askervein and is the value commonly adopted for the TU03-B benchmark.

Predicted velocities are sampled at the experimental A and AA stations at 10 m above local ground, as shown in Figure 2. These are compared against the experimental results, presented as the speedup compared to the incoming reference speed at 10 m height, which was 8.9 m/s for the experiment.

2.1.2 RESULTS

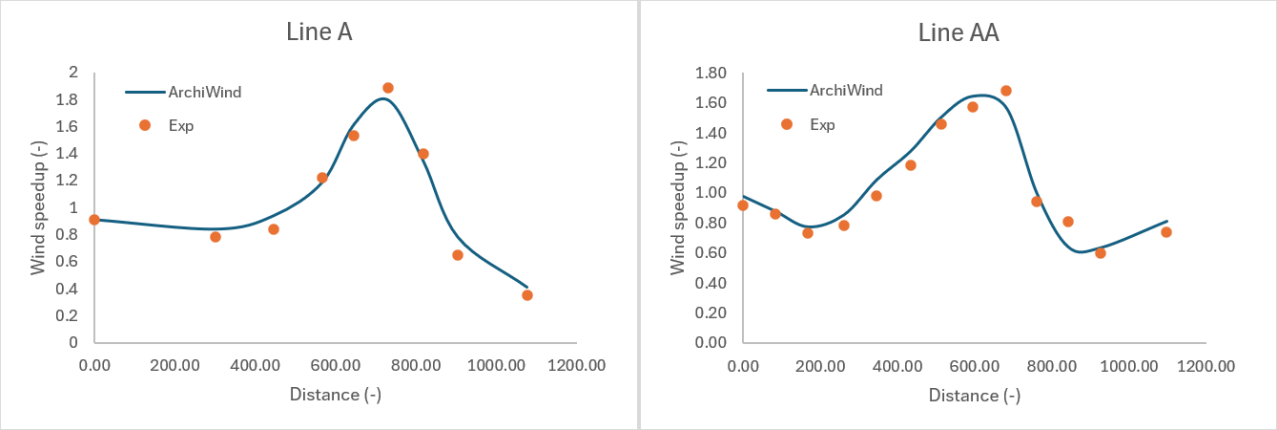


FIGURE 3 – COMPARISON BETWEEN FIELD SCALE DATA AND ARCHIWIND SIMULATION FOR LINE A AND LINE AA. DISTANCE IS MEASURED FROM THE FIRST MEASUREMENT PROBE.

The speedup of the ArchiWind simulation compared to the measured speedup along the two lines, Line A and Line AA that are aligned with the wind direction, is shown in Figure 3.

Both measurement lines show the characteristic response of a neutral atmospheric boundary layer passing over an isolated three-dimensional hill. The flow initially experiences a small reduction in velocity near the foot of the hill. It then accelerates rapidly along the upper windward slope, reaches its maximum speed near the crest, and decelerates strongly on the lee slope. This general behaviour is consistent with the original Askervein measurements and subsequent numerical studies, which show maximum speed-up close to the hilltop and minimum velocities in the lee of the hill.

The initial reduction in velocity can be associated with the pressure increase produced as the approaching atmospheric boundary layer encounters the hill. Farther up the windward slope, the pressure gradient becomes favourable and the streamlines are displaced upward and compressed. Conservation of mass through this reduced effective flow area produces a rapid increase in velocity. The strongest acceleration occurs over the upper slope and crest, where the surface pressure is relatively low and the streamlines are most strongly contracted.

Along line A, the normalized velocity is approximately 0.8 to 0.9 over the lower windward region before increasing sharply toward the crest. ArchiWind reproduces both the onset of the acceleration and the location and magnitude of the crest maximum reasonably well, although the calculated peak is slightly lower and smoother than the experimental value.

Immediately downstream of the line A crest, the velocity decreases very rapidly. The normalized experimental velocity falls from approximately 1.9 near the crest to approximately 0.65 farther down the lee slope and eventually to approximately 0.35 at the most downstream measurement location. This represents a strong lee-side velocity deficit. The decrease is caused by the adverse pressure gradient encountered after the crest, together with expansion of the streamlines and loss of near-surface momentum.

Along line AA, the same overall sequence is observed, but the flow response is somewhat less extreme. The normalized velocity first decreases to approximately 0.7 to 0.8, then rises progressively along the windward slope to a maximum of approximately 1.6 to 1.7 near CP. The lower maximum relative to line A is consistent with line AA crossing a lower or less strongly accelerating portion of the three-dimensional hill rather than the principal summit.

The line AA results also demonstrate the three-dimensional nature of the flow. In addition to moving over the terrain, part of the approaching flow is diverted laterally around the hill. The local acceleration therefore depends on both terrain elevation and the orientation of the slope relative to the approaching wind. This helps explain why the velocity distribution along line AA is broader and somewhat less sharply peaked than along line A.

Downstream of CP, the line AA velocity decreases to approximately 0.6. It then recovers to approximately 0.75 to 0.8 at the final location. This downstream recovery reflects turbulent transport of higher-momentum air from above and from the sides into the low-speed lee region. This part of the flow is the most sensitive to turbulence modelling, because the predicted velocity deficit depends strongly on turbulent mixing and the treatment of separation.

ArchiWind reproduces the principal features along line AA, including the initial windward deficit, progressive acceleration, crest maximum, sharp lee-side deceleration and subsequent recovery.

2.2 THE BOLUND HILL

The Bolund case [9] is a widely used validation benchmark for atmospheric flow over steep, complex terrain. Bolund is a small, isolated hill with an approximately 12 m elevation above the surrounding water and a particularly sharp escarpment on the western side. This abrupt change in terrain generates strong local acceleration over the crest and pronounced flow separation and recirculation in the lee, making the case considerably more demanding than smoother terrain benchmarks such as the Askervein hill from the previous section.

2.2.1 CASE DESCRIPTION AND CFD SETUP

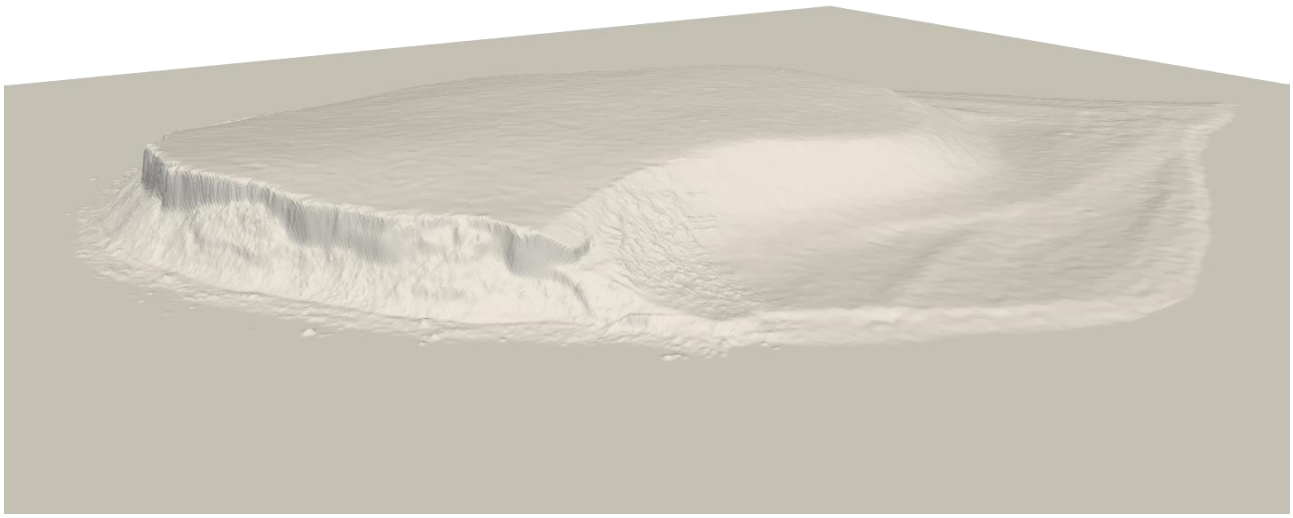


FIGURE 4 – 3D ORTHOGRAPHIC VIEW OF THE BOLUND HILL.

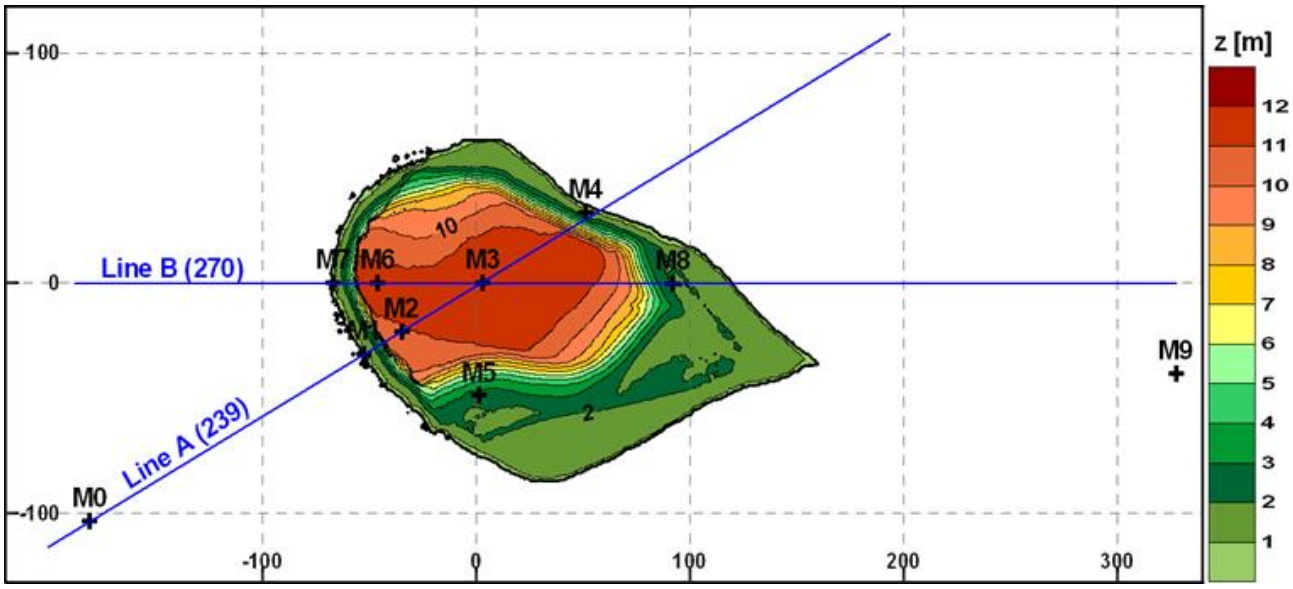


FIGURE 5 – LAYOUT OF EXPERIMENTAL MEASUREMENT MASTS.

Figure 4 shows the Bolund hill geometry. Figure 5 illustrates the position of the experimental measurement masts. For the current validation, the Line A masts are used for comparison, at elevation 5 m above ground level. Here, the flow direction is from 239 degrees. While the measurement points are sparse, they are positioned to capture the key flow phenomena of the flow over the hill, making it usable for comparison against CFD simulations.

2.2.2 RESULTS

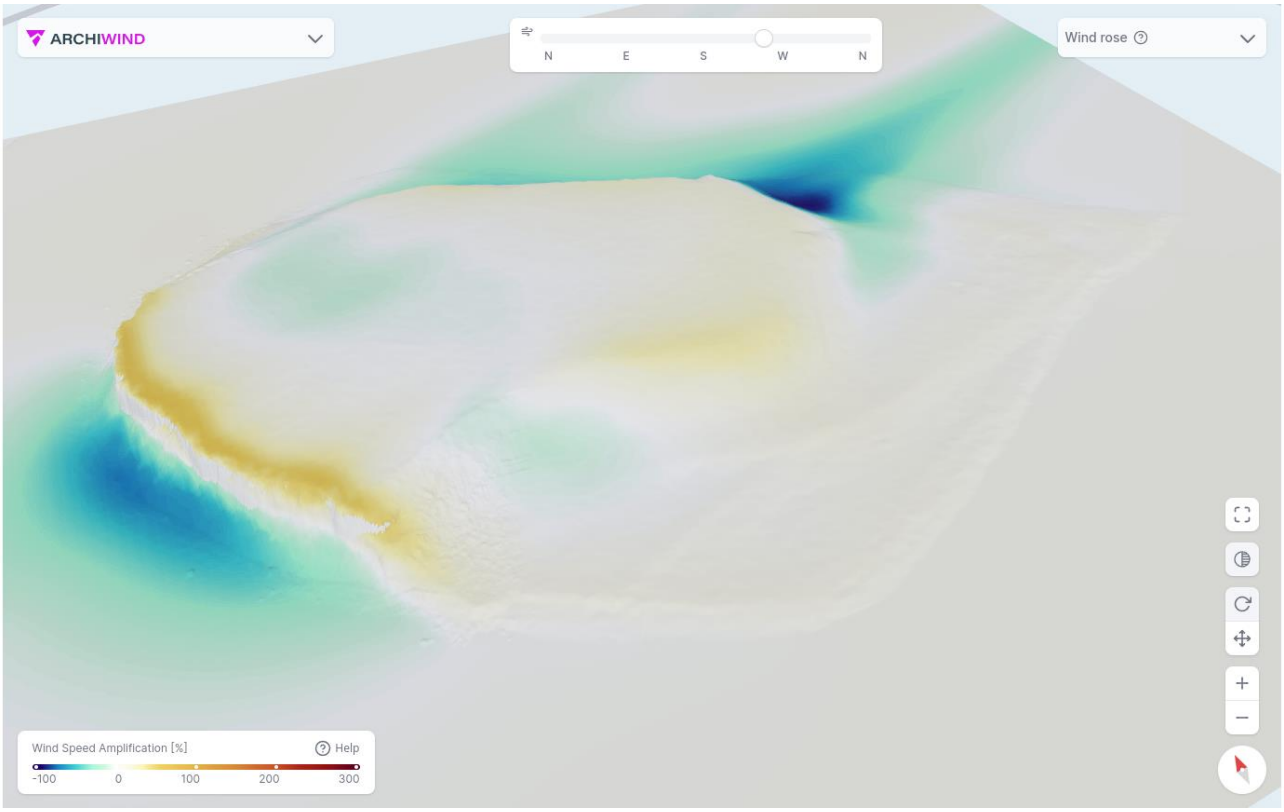


FIGURE 6 – VISUALIZATION OF WIND SPEED AMPLIFICATION, TAKEN FROM 1.5 M ABOVE GROUND LEVEL.

Figure 6 illustrates the overall flow field of the case. The flow field shown here is evaluated at 1.5 m above the local terrain surface and illustrates the characteristic response of the flow to the hill. Strong acceleration occurs along the exposed crest and escarpment, while substantial velocity deficits develop both immediately upstream and downstream of the steep terrain.

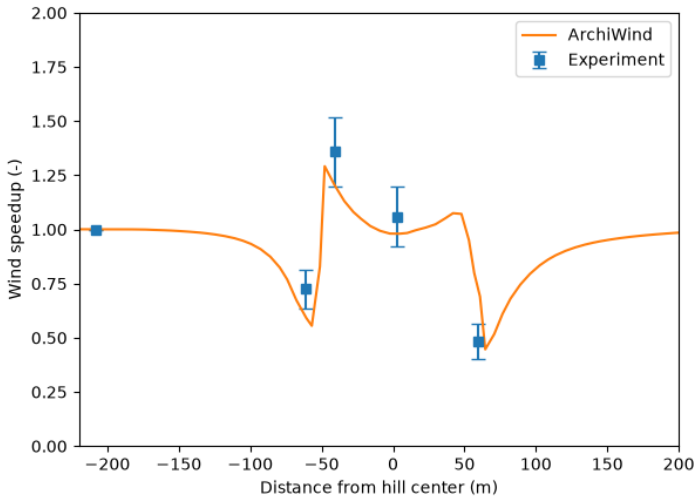


FIGURE 7 – COMPARISON BETWEEN ARCHIWIND SIMULATION AND EXPERIMENTS FOR THE BOLUND HILL CASE.

Figure 7 shows the speedup at the measurement points, compared against ArchiWind simulation results along Line A. This quantitative comparison shows good agreement between the ArchiWind predictions and the available experimental measurements along the transect. Despite the sparse measurement locations and the substantial experimental scatter, the simulation reproduces the principal features of the measured speed-up distribution. In particular, it captures the strong reduction in velocity approaching the steep upstream escarpment, the rapid acceleration close to the crest, and the subsequent reduction in speed in the downstream wake. The predicted values fall within the experimental uncertainty ranges, including in the regions where the flow changes rapidly over relatively short distances. The agreement is particularly encouraging because these locations are associated with strong terrain-induced pressure gradients, separation, and highly three-dimensional flow, all of which are challenging for steady RANS modelling. Overall, the results indicate that ArchiWind captures both the magnitude and spatial development of the terrain-induced speed-up with good accuracy for the Bolund benchmark.

3. FLOW IN URBAN ENVIRONMENTS

Accurate prediction of pedestrian-level wind speeds is a core requirement for urban wind comfort assessments. ArchiWind is a CFD platform built on the open-source software OpenFOAM and employs a steady-state Reynolds-Averaged Navier–Stokes (RANS) approach to predict pedestrian-level wind speed distributions. Validation against established benchmark datasets is essential to quantify the accuracy and reliability of the overall CFD modelling workflow and to build confidence in its use for engineering applications [6].

The AIJ Benchmark Case E represents the urban area surrounding the Niigata Meteorological Observatory and is one of the most demanding test cases in the AIJ suite: it features a dense irregular urban geometry, 16 wind directions, and a paired before/after construction dataset that allows explicit evaluation of a solver's ability to detect the wind impact of a new building [1].

This section is structured as follows:

Section 3.1 describes the case geometry, measurement setup, and CFD configuration.

Section 3.2 presents results for the After-construction scenario vs. experiment.

Section 3.3 presents results for the Before construction scenario vs. experiment.

Section 3.4 evaluates whether ArchiWind detects the wind changes caused by the new building.

Section 3.5 compares Detailed and Draft mesh quality for the After scenario.

Section 3.6 compares the k-ε and k-ω SST turbulence models for the After scenario.

Appendices A–D report line plots for all 16 wind directions.

3.1. CASE DESCRIPTION AND CFD SETUP

3.1.1 NIIGATA URBAN ENVIRONMENT

Case E represents a 500 × 500 m area of the Niigata city centre, modelled at a 1:1000 scale in the wind tunnel. The domain includes a dense arrangement of low- to mid-rise buildings with irregular plan shapes. Measurements were conducted at 80 pedestrian-level probe points (z = 2 m full scale) for 16 wind directions (N, NNE, NE, … NNW, at 22.5° intervals).

The dataset is provided in two versions: Before-Construction (existing urban fabric) and After-Construction (same fabric with additional buildings). Comparing the two configurations allows assessment of ArchiWind's ability to resolve the localised wind impact of a new structure.



FIGURE 8 - CASE E GEOMETRY WITH THE 80 PEDESTRIAN-LEVEL PROBE POINT LOCATIONS. POINTS ARE LOCATED AT Z = 2 M (FULL SCALE).

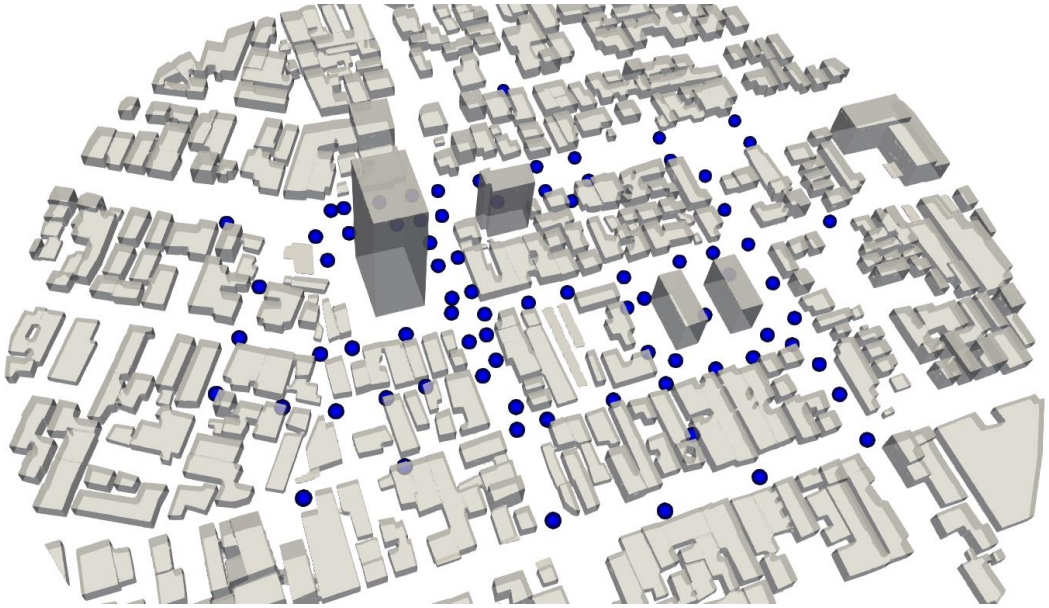


FIGURE 9 - 3D VIEW OF THE CASE E URBAN GEOMETRY WITH THE 80 PEDESTRIAN-LEVEL PROBE POINTS (BLUE DOTS) SHOWN IN THEIR SPATIAL ARRANGEMENT.

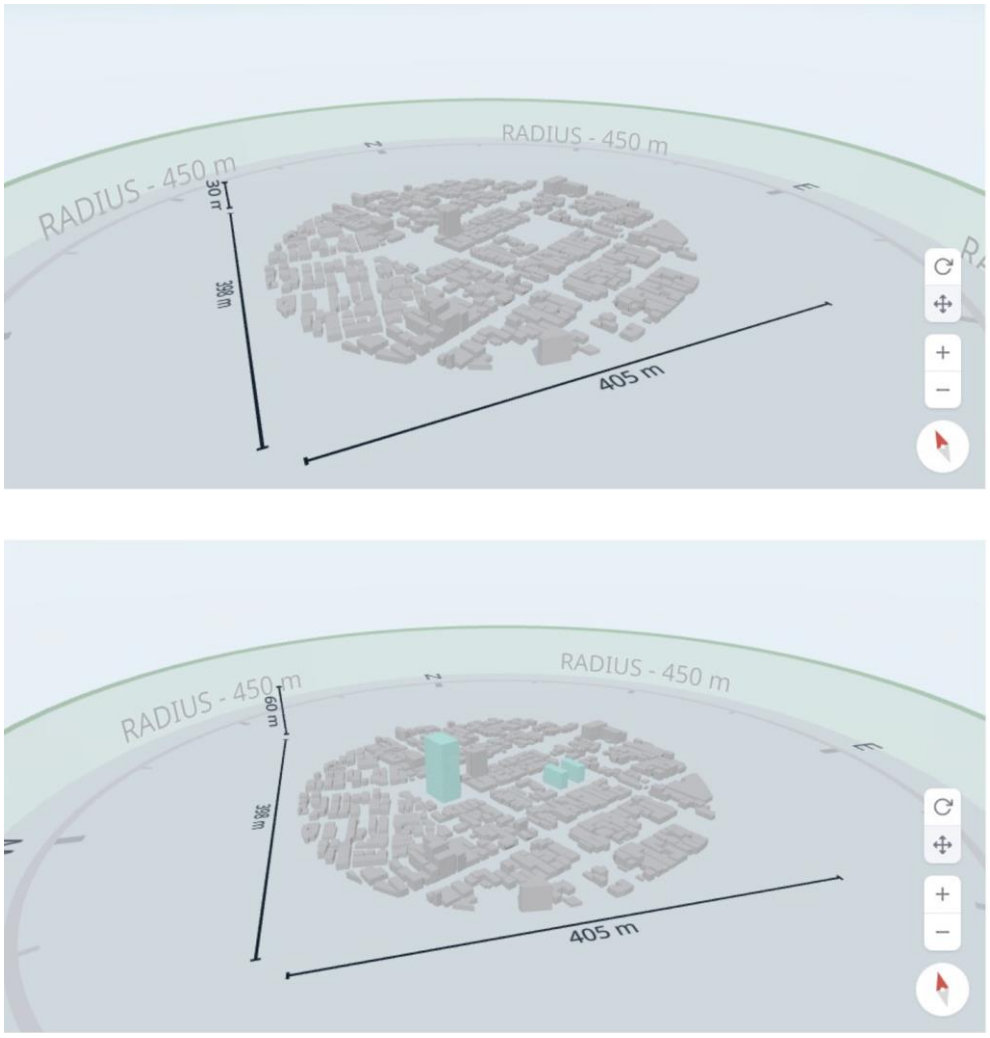


FIGURE 10 - ARCHIWIND COMPUTATIONAL DOMAIN — BEFORE-CONSTRUCTION (TOP) AND AFTER-CONSTRUCTION (BOTTOM).

3.1.2 COMPUTATIONAL DOMAIN

Mesh generation and boundary condition assignment are handled automatically by ArchiWind's preprocessing pipeline. The computational domain adopts a circular layout. Results are evaluated within an inner zone of radius 5H from the building cluster, where H is the height of the tallest building, in accordance with AIJ guidelines [2] and best-practice recommendations [5]. The domain configuration follows the approach of Hågbo and Giljarhus [7]. Mesh resolution was set following the same guidelines.

ArchiWind employs a cylindrical domain geometry, following the approach of Hågbo and Giljarhus [7], which allows the same mesh to be used for any wind direction. While AIJ best-practice guidelines [2] specify distinct inlet and outlet distances for box-shaped domains, these recommendations assume a fixed inlet direction and are not directly applicable to multi-direction studies. In the cylindrical configuration, the radial distance from the building cluster to the domain boundary is set to 15H in all directions [7] — consistent with the AIJ 15H outlet requirement — ensuring that the inlet boundary is placed well away from the region of influence of the buildings for all 16 simulated wind directions.

3.1.3 TURBULENCE MODELS

Two RANS turbulence models were evaluated:

Realizable k-ε (production model): a well-established model for bluff-body flows, featuring improved predictions of spreading rates and recirculation zones compared to the standard k-ε formulation [3].

k-ω SST (comparison model): a hybrid model combining k-ω near walls and k-ε in the free stream, often recommended for flows with adverse pressure gradients [4].

3.1.4 INLET BOUNDARY CONDITION AND REFERENCE VELOCITY

In standard applications, ArchiWind automatically derives atmospheric boundary layer profiles from upstream terrain roughness for each wind direction. For this benchmark, prescribed roughness parameters were used to reproduce the inflow conditions reported in the AIJ wind tunnel dataset [1].

The inlet velocity and turbulence profiles were prescribed from the AIJ-published wind tunnel inflow measurements. The reference velocity U_ref = 3.928 m/s is defined at z = 15.9 m (height of the Niigata meteorological station), consistent with the AIJ normalization convention.

To verify that the inlet profile is preserved through the fetch region upstream of the measurement area, an ABL profile check was performed at distances of 220 m to 900 m upstream of the building cluster. The figure below shows the velocity profile at each fetch distance compared to the AIJ target.

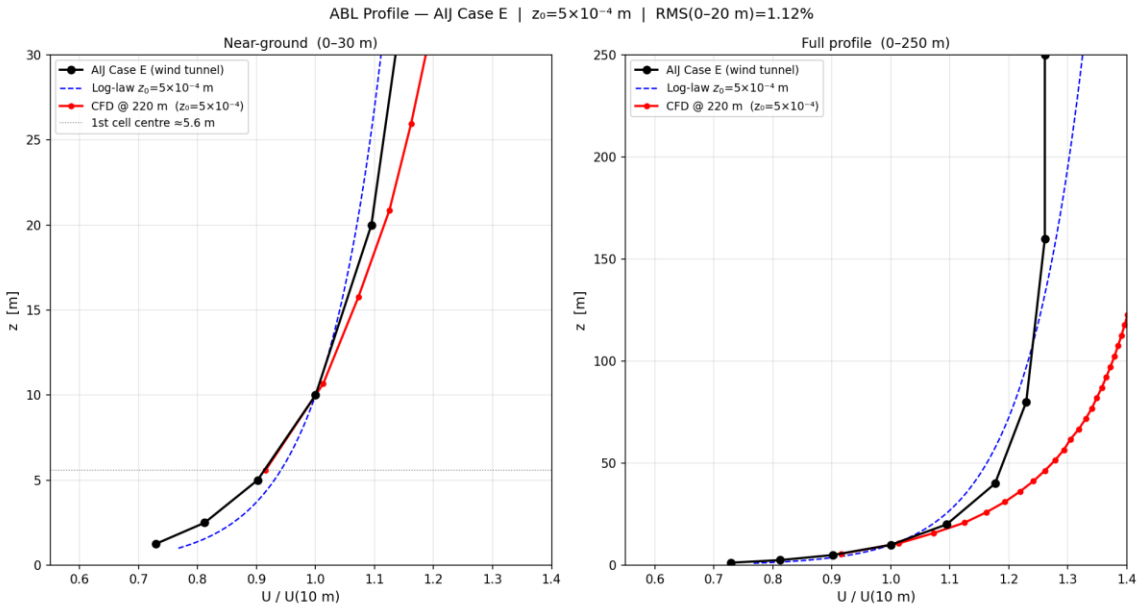


FIGURE 11 - FETCH PROFILE ANALYSIS: SIMULATED ABL VELOCITY PROFILE AT MULTIPLE UPSTREAM DISTANCES VS. THE AIJ TARGET INFLOW. THE 220 M UPSTREAM PROFILE IS USED AS THE NORMALIZATION REFERENCE.

3.1.5 VALIDATION METRIC

The primary quantity of comparison is the normalized scalar wind speed $Vs\ /\ U_ref\ = \sqrt{(Ux^2\ +\ Uy^2\ +\ Uz^2)}\ /\ U_ref$, which is directly comparable to the normalised values provided by the AIJ datasets. Performance is quantified by three metrics computed over all N available measurement points, where CFD_i and Exp_i denote the normalized wind speed predicted and measured at probe i:

RMSE: root mean square error of the normalized wind speed

$$RMSE = \sqrt{\frac{\sum(CFD_i - Exp_i)^2}{N}}$$

Bias: systematic over- or underprediction averaged across all probes. Positive means CFD overestimates, negative means CFD underestimates.

$$Bias\ = \frac{1}{N}\sum(CFD_i\ -\ Exp_i)$$

$\mathbf{R^2}$: spatial correlation between CFD and experiment: $\mathbf{R}^2\ = 1$ indicates perfect agreement, $\mathbf{R}^2\ = 0$ means the CFD has no predictive power for the spatial wind pattern, $\mathbf{R}^2\ < 0$ means it performs worse than simply predicting the spatial mean.

$$R^2 = 1\ -\ \frac{\sum(CFD_i\ -\ Exp_i)^2}{\sum(Exp_i\ -\ \bar{E})^2}$$

where $\bar{E}$ is the mean of the experimental values.

3.2 AFTER-CONSTRUCTION VS. EXPERIMENT

This section compares ArchiWind results for the After-Construction configuration (Detailed mesh quality) against wind tunnel measurements.

3.2.1 GLOBAL ACCURACY

Figure 9 shows the global scatter plot pooling all 80 probe points and 16 wind directions. The dashed line represents perfect agreement.

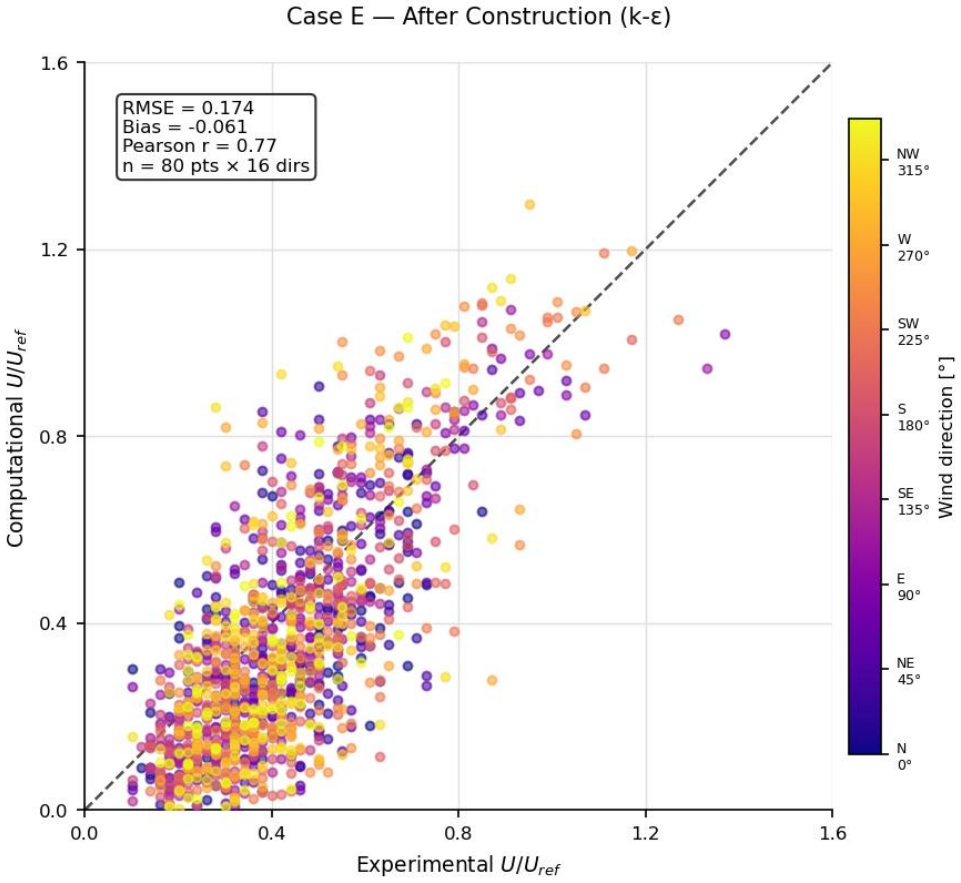


FIGURE 12 - GLOBAL SCATTER — AFTER-CONSTRUCTION: EXPERIMENTAL (X) VS. COMPUTATIONAL (Y) NORMALISED WIND SPEED U/U_REF. ALL 80 POINTS × 16 DIRECTIONS. DASHED LINE = PERFECT AGREEMENT.

Table 1 reports the global validation metrics:

Configuration	N pts	N dirs	RMSE	Bias	Pearson r
After — Detailed	80	16	0.174	-0.061	0.769

Table 1. *Global validation metrics — Case E, After-Construction.*

3.2.2 RESULTS BY CARDINAL DIRECTION

Figure 13 and Figure 14 show line plots and scatter plots for the four cardinal wind directions (N, E, S, W). Each line plot displays ArchiWind (blue solid) and experiment (grey dashed) across all 80 probe points. Results for all 16 directions are provided in Appendix A.



FIGURE 13 - LINE PLOTS — AFTER-CONSTRUCTION, CARDINAL DIRECTIONS. GREY DASHED: EXPERIMENT. BLUE SOLID: ARCHIWIND. RMSE AND PEARSON R ARE SHOWN FOR EACH DIRECTION.

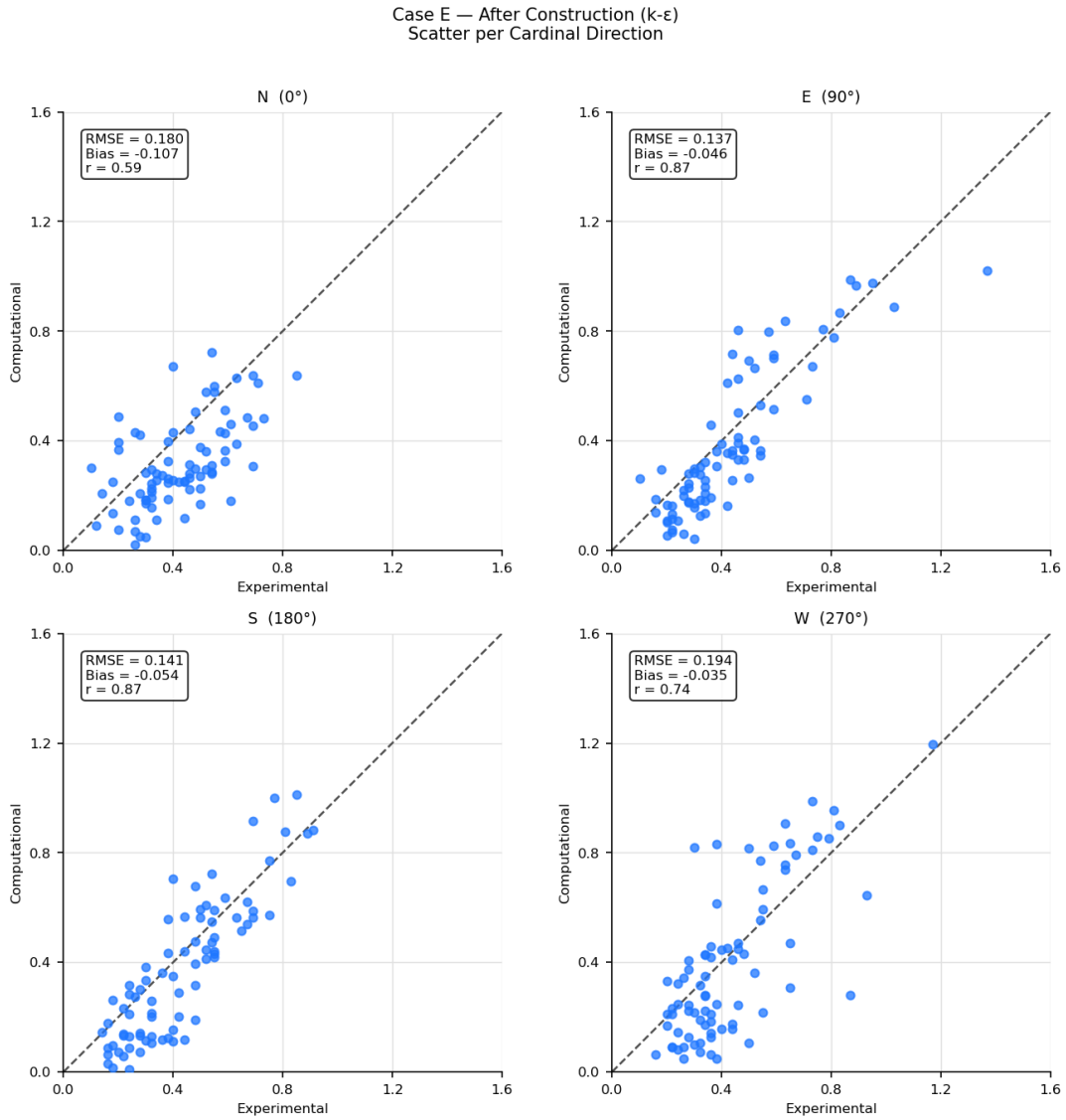


FIGURE 14 - SCATTER PLOTS PER CARDINAL DIRECTION — AFTER-CONSTRUCTION. X-AXIS: EXPERIMENTAL. Y-AXIS: COMPUTATIONAL.

3.2.3 ERROR ANALYSIS

Figure 15 shows RMSE and bias for each of the 16 wind directions. Figure 16 shows the velocity field at pedestrian level for the North wind direction, giving a qualitative view of the CFD output.

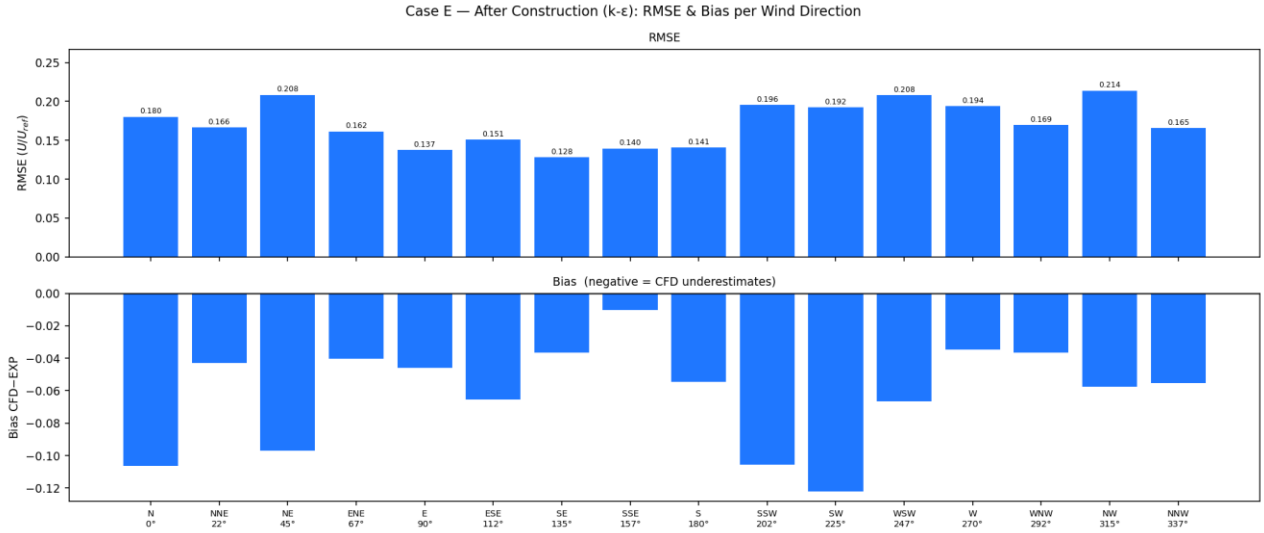


FIGURE 15 – RMSE AND BIAS PER WIND DIRECTION — AFTER-CONSTRUCTION.

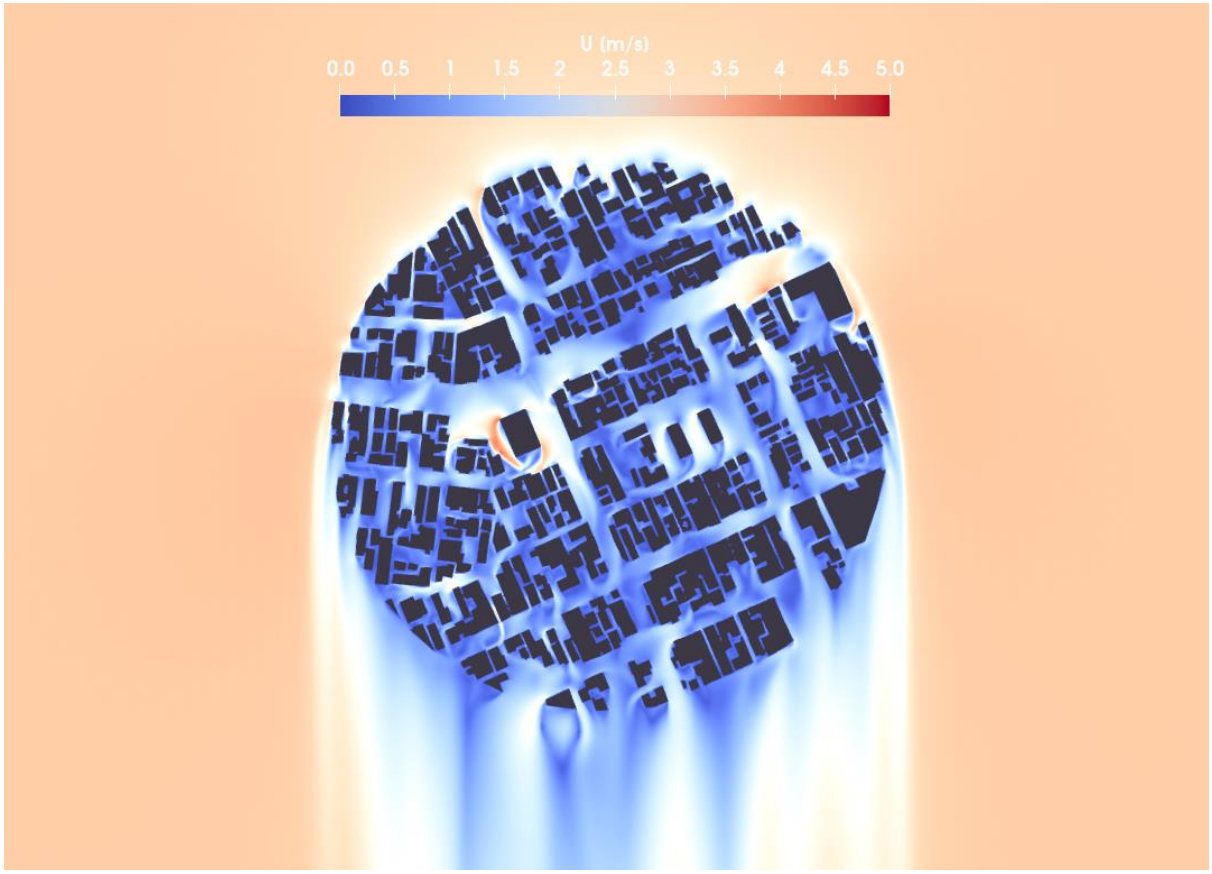


FIGURE 16 – VELOCITY FIELD U AT PEDESTRIAN LEVEL — AFTER-CONSTRUCTION, NORTH WIND DIRECTION (0°). BLUE INDICATES SHELTERED ZONES; RED COLOURS INDICATE ACCELERATED FLOW.

3.3 BEFORE CONSTRUCTION VS. EXPERIMENT

This section compares ArchiWind results for the Before-Construction configuration against wind tunnel measurements of the original urban fabric.

3.3.1 GLOBAL ACCURACY

Figure 17 shows the global scatter for the Before configuration.

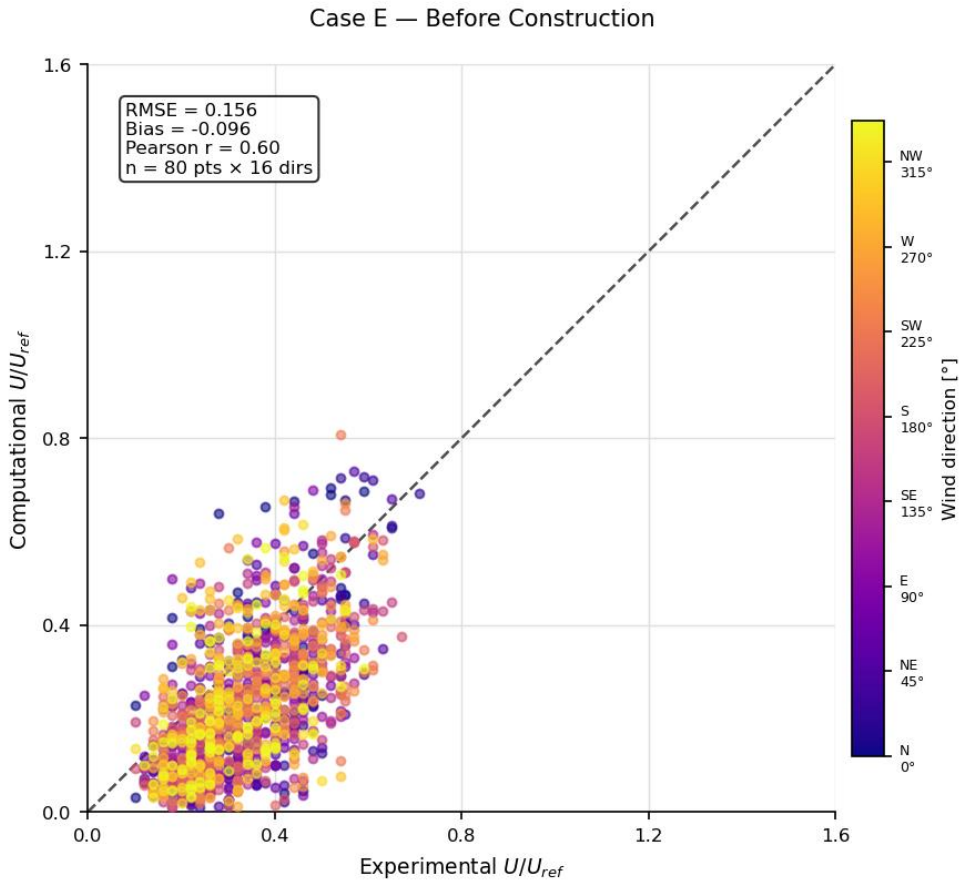


FIGURE 17 - GLOBAL SCATTER — BEFORE-CONSTRUCTION: EXPERIMENTAL (X) VS. COMPUTATIONAL (Y) NORMALISED WIND SPEED. ALL 80 POINTS × 16 DIRECTIONS.

Table 2 reports the global validation metrics:

Configuration	N pts	N dirs	RMSE	Bias	Pearson r
Before — Detailed	80	16	0.156	-0.096	0.603

Table 2. *Global validation metrics — Case E, Before-Construction.*

3.3.2 RESULTS BY CARDINAL DIRECTION

Figure 18 and Figure 19 show line plots and scatter plots for the cardinal directions. Results for all 16 directions are provided in Appendix B.



FIGURE 18 - LINE PLOTS — BEFORE-CONSTRUCTION, CARDINAL DIRECTIONS. GREY DASHED: EXPERIMENT. BLUE SOLID: ARCHIWIND.

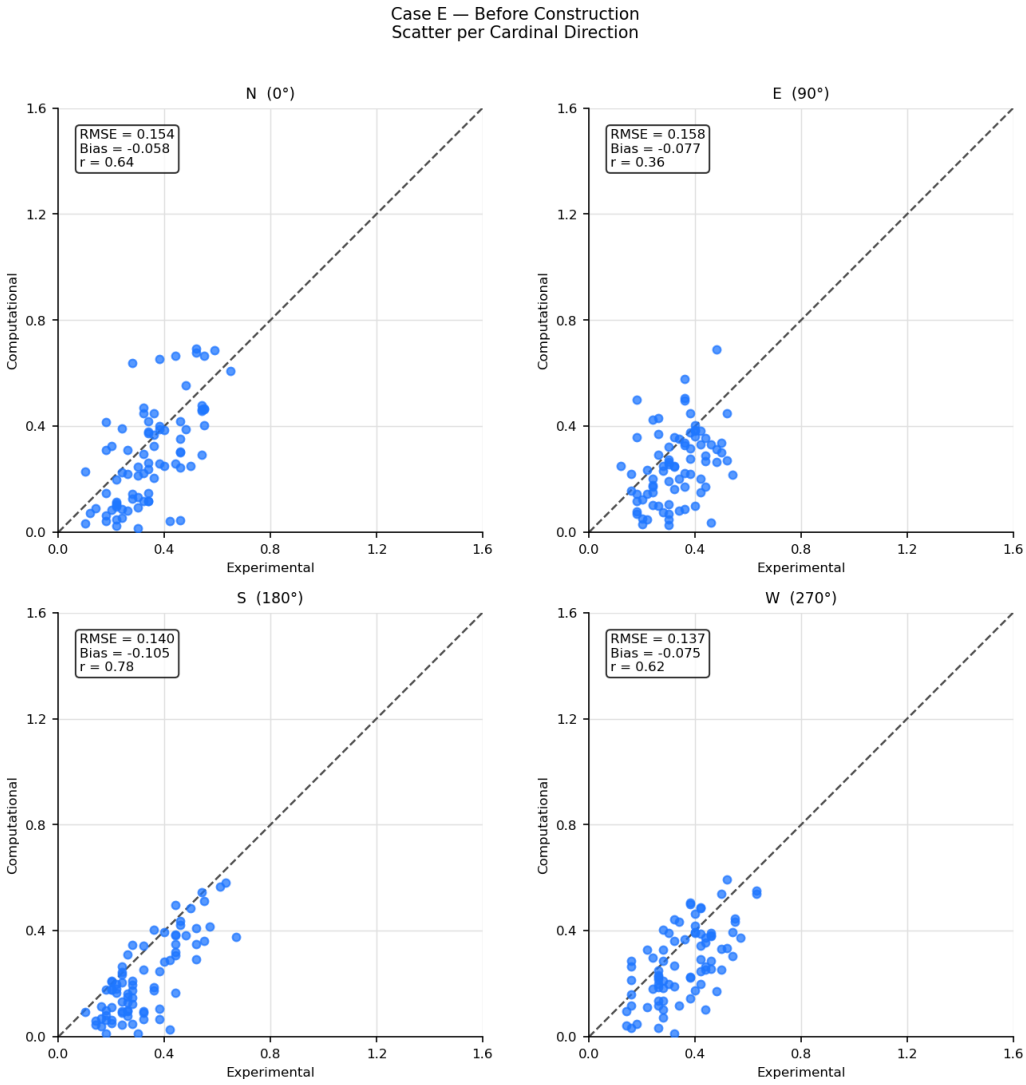


FIGURE 19 – A SCATTER PLOTS PER CARDINAL DIRECTION — BEFORE-CONSTRUCTION.

3.3.3 ERROR ANALYSIS

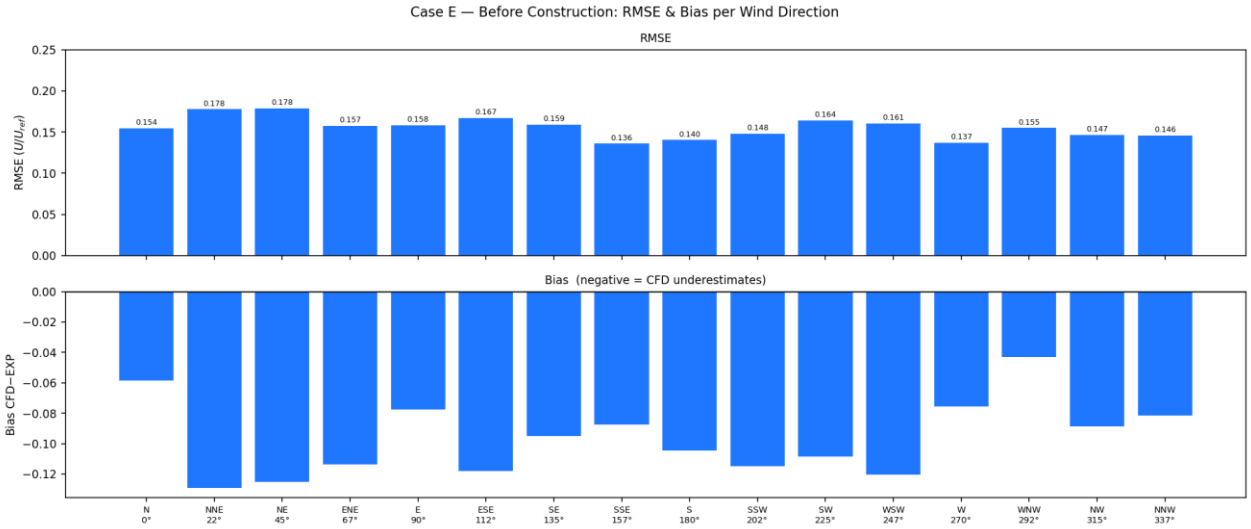


FIGURE 20 – RMSE AND BIAS PER WIND DIRECTION — BEFORE-CONSTRUCTION.

3.4. CONSTRUCTION EFFECT

A key use case for ArchiWind is assessing the wind impact of a new building on the surrounding pedestrian environment. This section evaluates whether the CFD-predicted change in wind speed (ΔU = After − Before) matches the change measured in the wind tunnel.

3.4.1 BEFORE VS. AFTER

Figure 21 places the two global scatter plots side by side to illustrate how the overall accuracy compares between configurations.

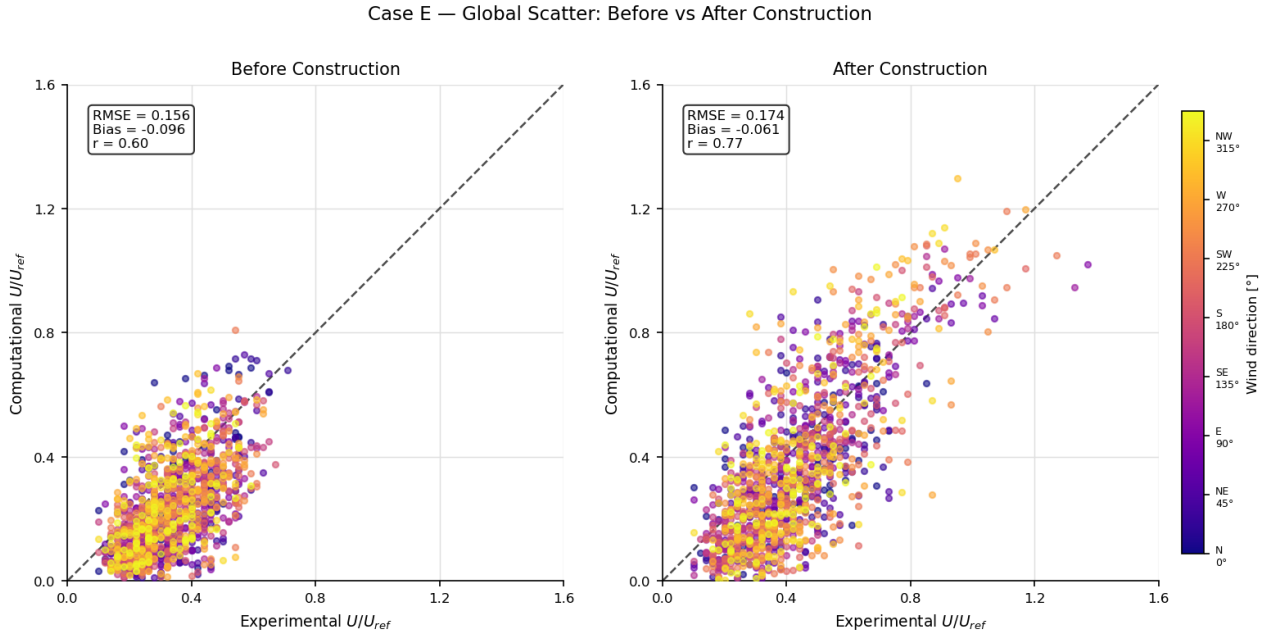


FIGURE 21 - GLOBAL SCATTER — BEFORE (LEFT) AND AFTER (RIGHT) CONSTRUCTION. AXES: EXPERIMENTAL (X) VS. COMPUTATIONAL (Y).

3.4.2 ΔU SCATTER AND SPATIAL MAPS

Figure 22 shows the scatter of CFD-predicted ΔU vs. experimentally measured ΔU for all 80 points and 16 wind directions, coloured by wind direction, together with spatial maps of mean ΔU per probe point averaged over all 16 directions.

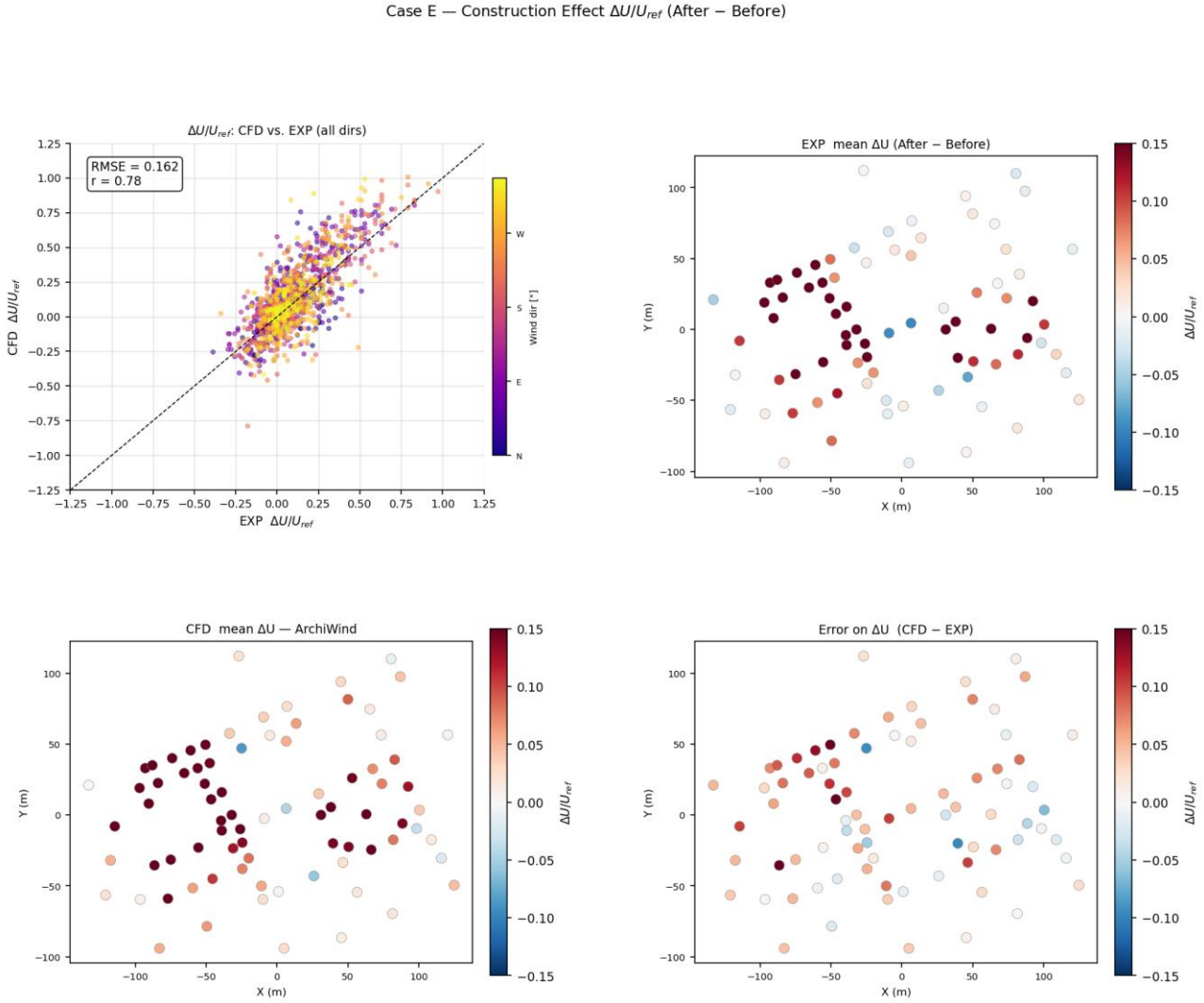


FIGURE 22 - CONSTRUCTION EFFECT ΔU/U_REF (AFTER – BEFORE). TOP-LEFT: SCATTER CFD VS. EXP COLOURED BY WIND DIRECTION. TOP-RIGHT: EXPERIMENTAL MEAN ΔU PER PROBE. BOTTOM-LEFT: ARCHIWIND MEAN ΔU. BOTTOM-RIGHT: ERROR ON ΔU (CFD – EXP). SPATIAL MAPS AVERAGED OVER 16 WIND DIRECTIONS.

A positive ΔU indicates wind speed increase due to the new building (channelling effect); negative values indicate sheltering. The scatter confirms that ArchiWind correctly identifies the sign and approximate magnitude of the construction effect at most probe locations.

3.4.3 MEAN VELOCITY AND RESIDUAL MAPS

Figure 23 and Figure 24 provide spatial context by showing the mean velocity ratio averaged over all 16 directions, and the mean residual per probe point.

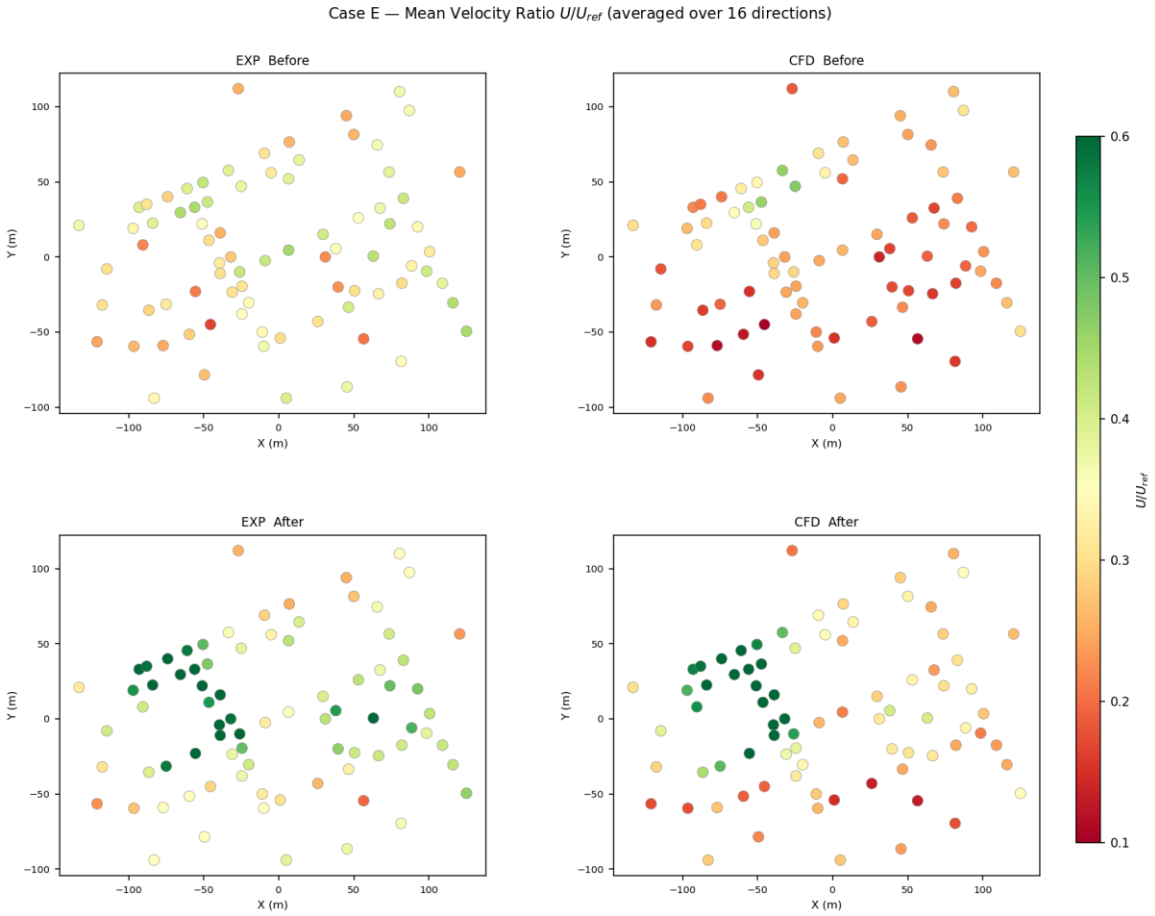


FIGURE 23 - SPATIAL MAP OF MEAN NORMALISED WIND SPEED U/U_REF (AVERAGED OVER 16 DIRECTIONS). ROWS: BEFORE (TOP) / AFTER (BOTTOM). COLUMNS: EXPERIMENT (LEFT) / ARCHIWIND (RIGHT).

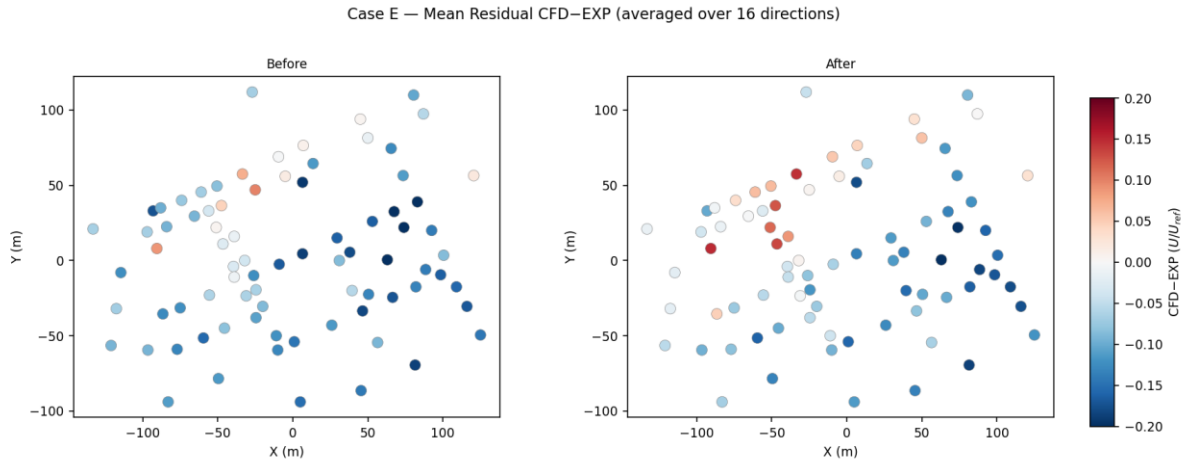


FIGURE 24 - MEAN RESIDUAL CFD – EXP PER PROBE POINT (AVERAGED OVER 16 DIRECTIONS). LEFT: BEFORE. RIGHT: AFTER. RED = CFD OVERESTIMATES; BLUE = CFD UNDERESTIMATES.

3.5 MESH QUALITY: DETAILED VS DRAFT

ArchiWind offers two mesh quality settings: Detailed and Draft. The Detailed setting uses a finer mesh with tighter near-wall refinement around buildings, while Draft uses a coarser mesh for faster run times. Figure 25 shows the mesh cross-section for each setting. This section quantifies the impact of mesh quality on prediction accuracy for the After-construction configuration.

It should be noted that for this validation study, the Draft simulation was run using all 16 wind directions to match the full set of experimental directions available in the AIJ dataset. In standard ArchiWind applications, the Draft setting simulates only 8 wind directions, reducing computation time while still covering the principal flow directions [7]. The results presented in this section therefore assess mesh quality independently of the reduced direction set. While the CFD predictions are shown to be reliable, a standard Draft study will be less exhaustive than a Detailed study in practice, as fewer wind directions are evaluated.

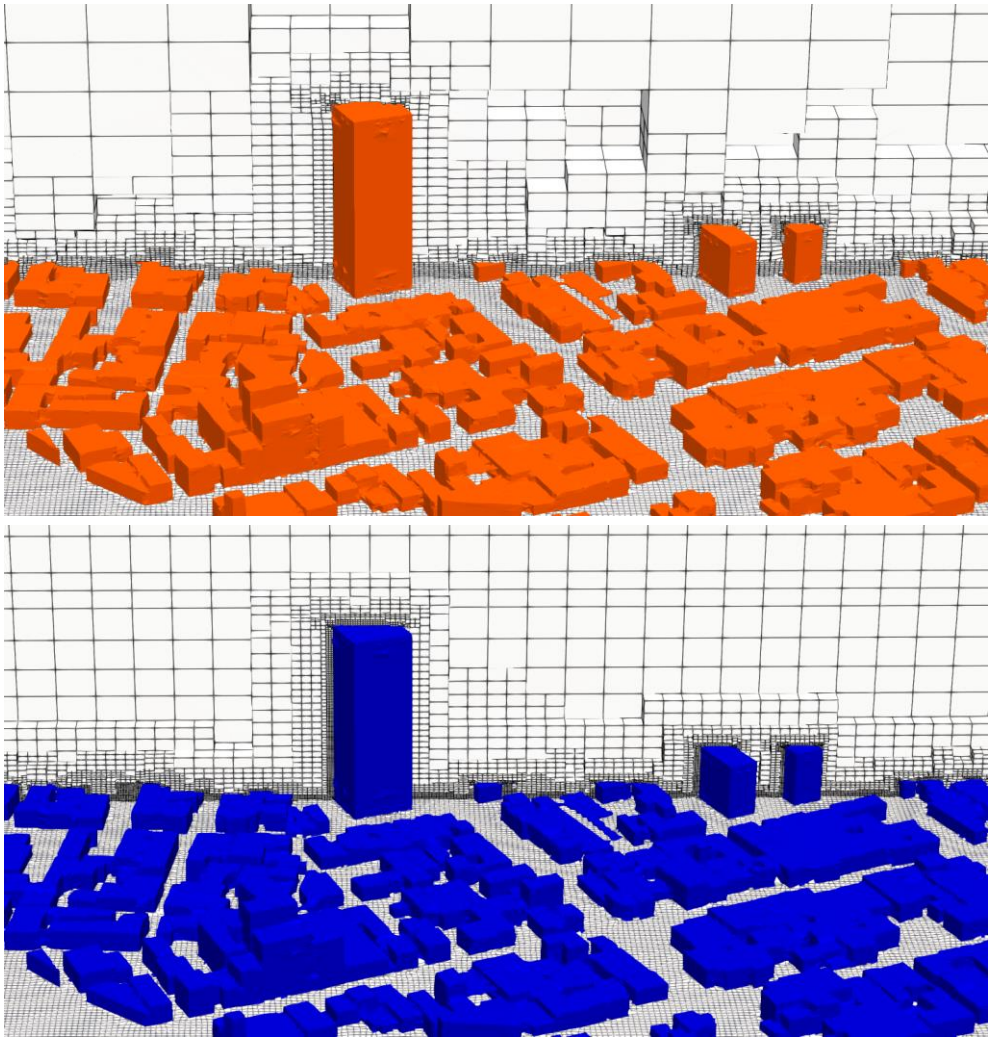


FIGURE 25 - MESH CROSS-SECTION — DRAFT (TOP) AND DETAILED (BOTTOM) QUALITY SETTING.

3.5.1 GLOBAL ACCURACY

Figure 26 shows the global scatter for both mesh quality levels side by side.

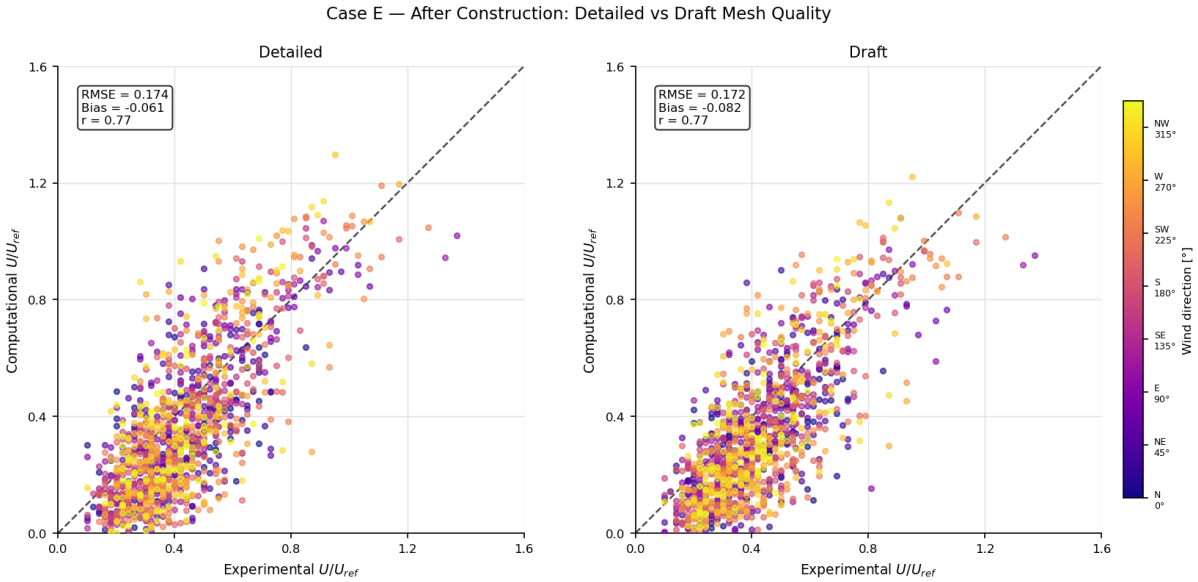


FIGURE 26 – GLOBAL SCATTER — DETAILED (LEFT) VS. DRAFT (RIGHT) MESH QUALITY, AFTER-CONSTRUCTION. AXES: EXPERIMENTAL (X) VS. COMPUTATIONAL (Y).

Table 3 summaries the metrics for both quality levels:

Mesh Quality	RMSE	Bias	Pearson r
Detailed	0.174	-0.061	0.769
Draft	0.172	-0.082	0.769

Table 3. *Metric comparison — Detailed vs. Draft mesh quality, After-Construction.*

3.5.2 RESULTS BY CARDINAL DIRECTION

Figure 27 overlays Detailed and Draft results on the same line plots for the four cardinal directions, allowing direct point-by-point comparison. Figure 28 shows the RMSE and bias per direction for both quality settings.

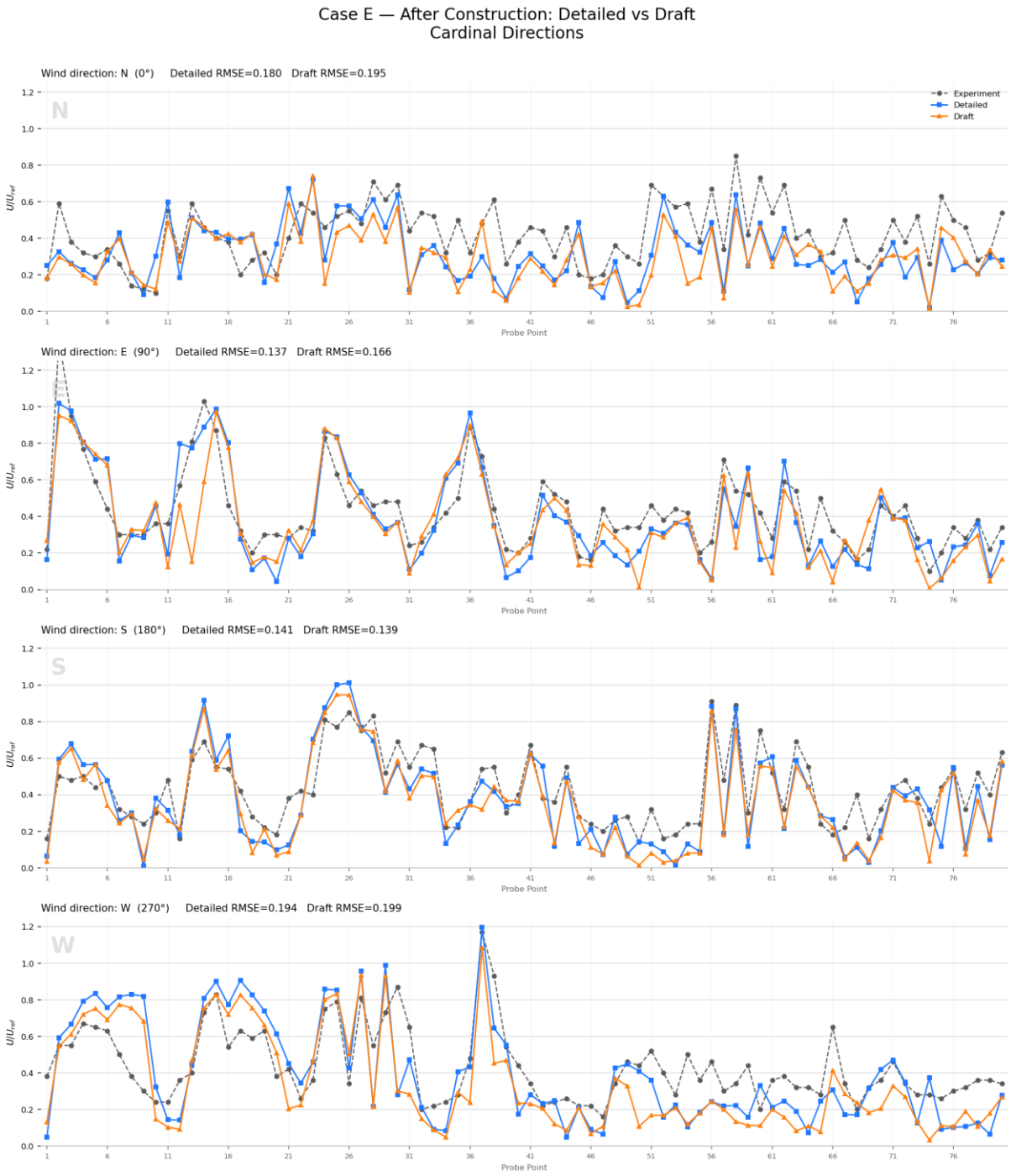


FIGURE 27 - LINE PLOTS — AFTER-CONSTRUCTION, CARDINAL DIRECTIONS: EXPERIMENT (GREY DASHED), DETAILED (BLUE), DRAFT (ORANGE). RMSE SHOWN PER DIRECTION FOR EACH QUALITY SETTING.

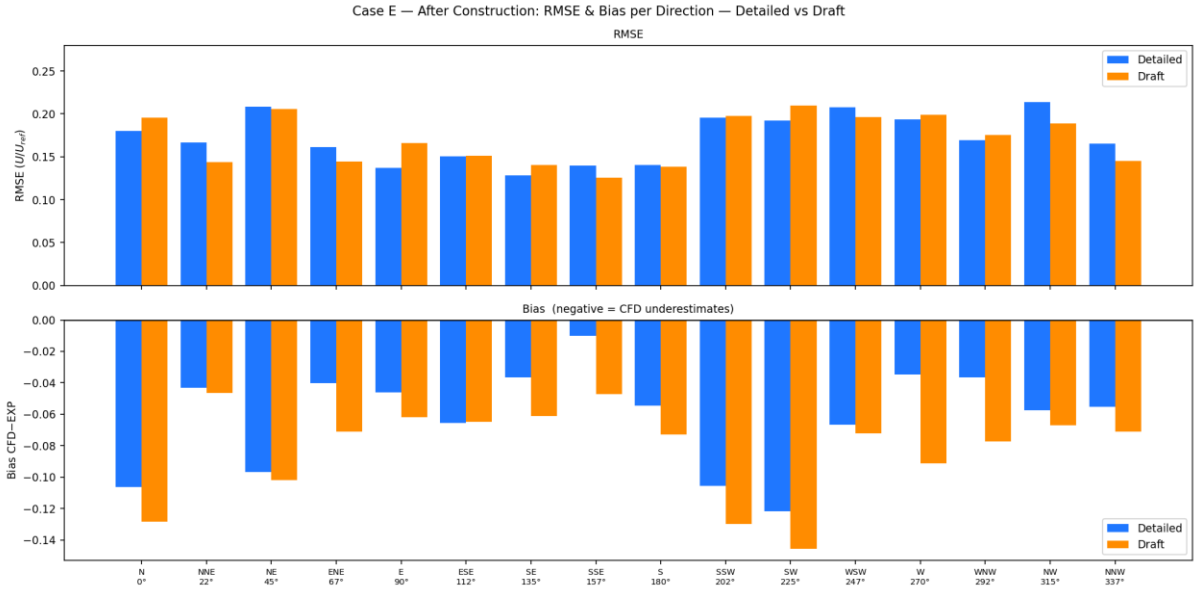


FIGURE 28 - RMSE AND BIAS PER WIND DIRECTION: DETAILED (BLUE) VS. DRAFT (ORANGE).

3.5.3 ERROR DISTRIBUTION

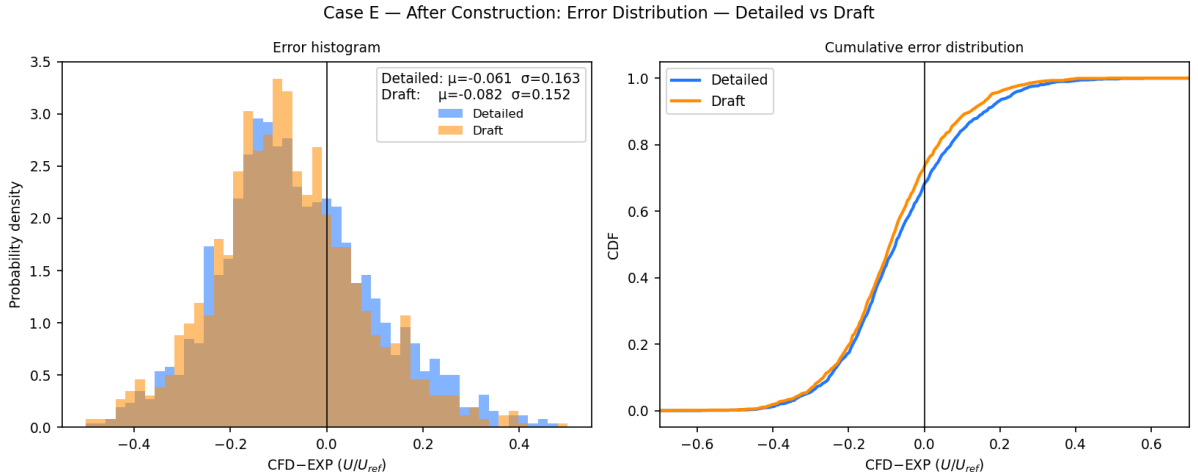


FIGURE 29 - ERROR DISTRIBUTION (CFD – EXP) — DETAILED (BLUE) VS. DRAFT (ORANGE). LEFT: HISTOGRAM. RIGHT: CUMULATIVE DISTRIBUTION.

Results for all 16 wind directions (Draft quality) are provided in Appendix C.

3.6 TURBULENCE MODEL COMPARISON

This section compares the Realizable k-ε model used in the preceding sections against the k-ω SST model for the After-construction configuration. Both simulations use the same Detailed mesh and boundary conditions; only the turbulence model differs.

3.6.1 GLOBAL ACCURACY

Figure 30 shows the global scatter for both turbulence models side by side.

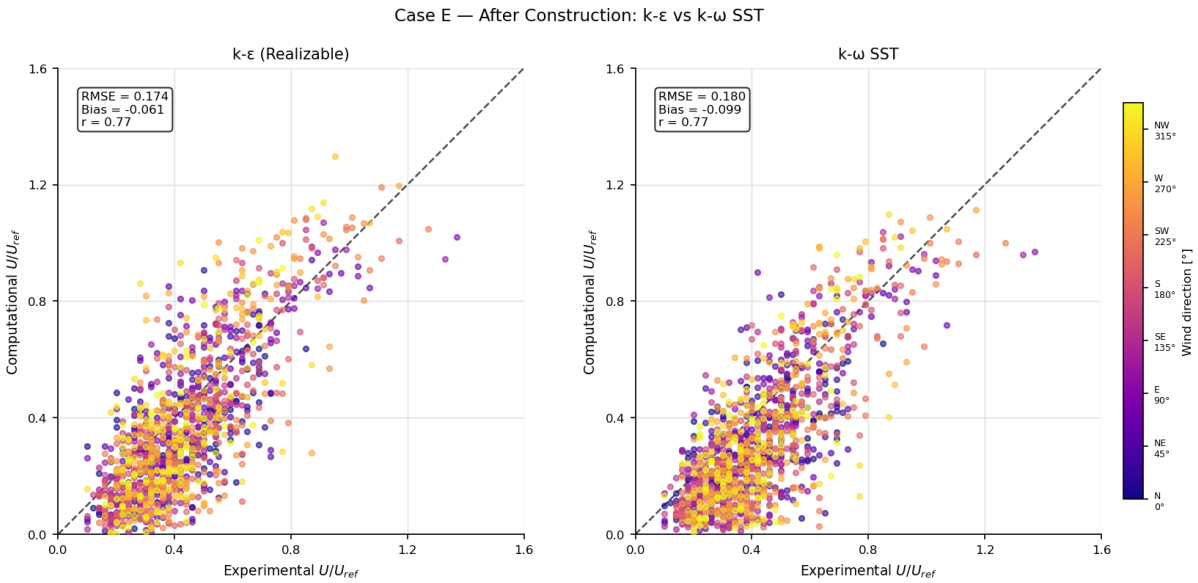


FIGURE 30 - GLOBAL SCATTER —REALIZABLE K -E (LEFT) VS. K-Ω SST (RIGHT), AFTER CONSTRUCTION. AXES: EXPERIMENTAL (X) VS. COMPUTATIONAL (Y). POINTS COLOURED BY WIND DIRECTION.

Table 4 summarizes the global metrics for both models:

Turbulence Model	RMSE	Bias	Pearson r
k-ε (Realizable)	0.174	-0.061	0.769
k-ω SST	0.180	-0.099	0.771

Table 4. *Global validation metrics — Realizable k-ε vs k-ω SST, After construction.*

3.6.2 RESULTS BY CARDINAL DIRECTION

Figure 31 overlays k-ε and k-ω SST results on the same line plots for the four cardinal directions. Figure 32 shows the RMSE and bias per direction for both models. Results for all 16 wind directions are provided in Appendix D.

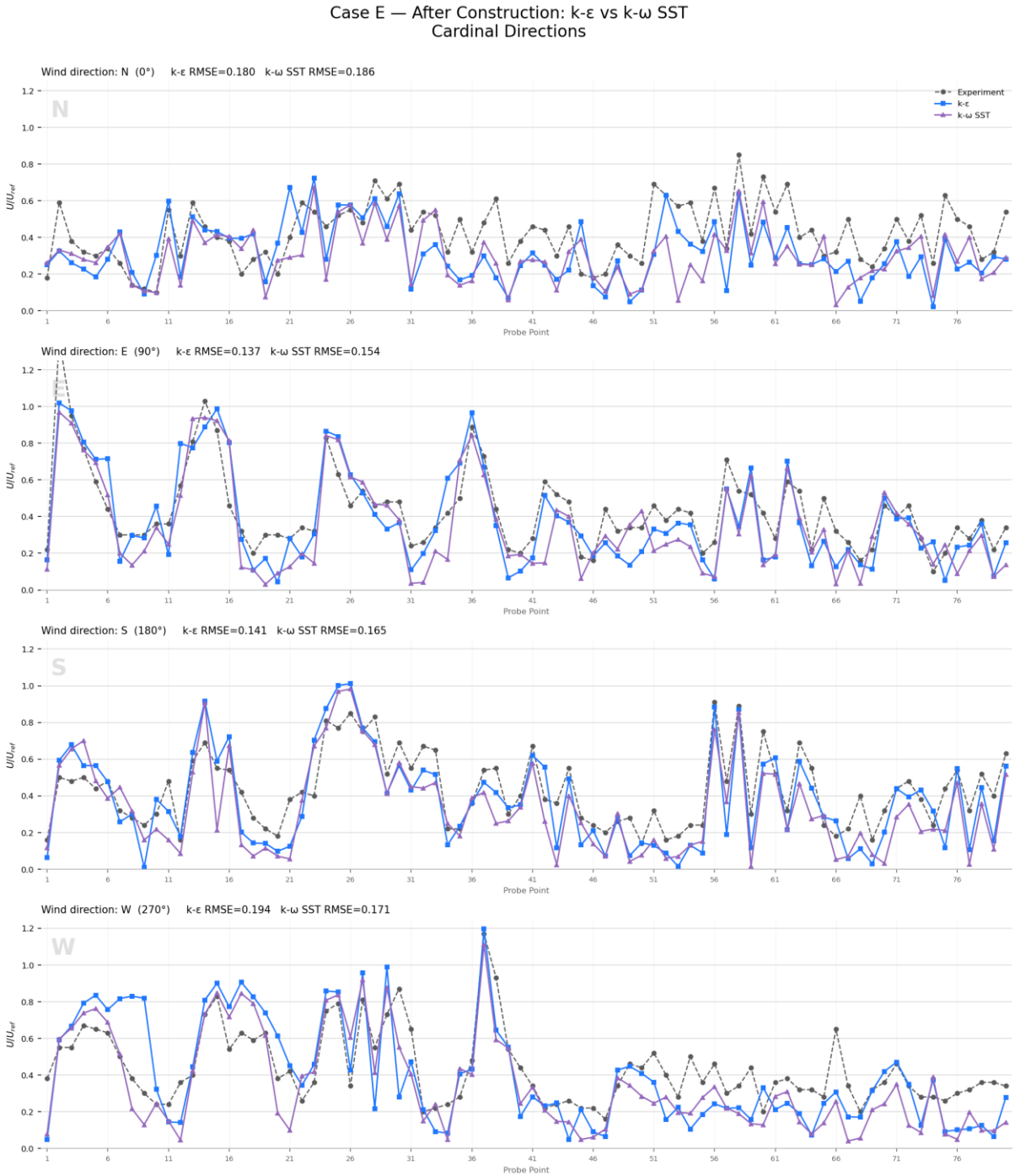


FIGURE 31 - LINE PLOTS — AFTER CCONSTRUCTION, CARDINAL DIRECTIONS: EXPERIMENT (GREY DASHED),REALIZABLE K-E (BLUE), K-Ω SST (PURPLE). RMSE SHOWN PER DIRECTION FOR EACH MODEL.

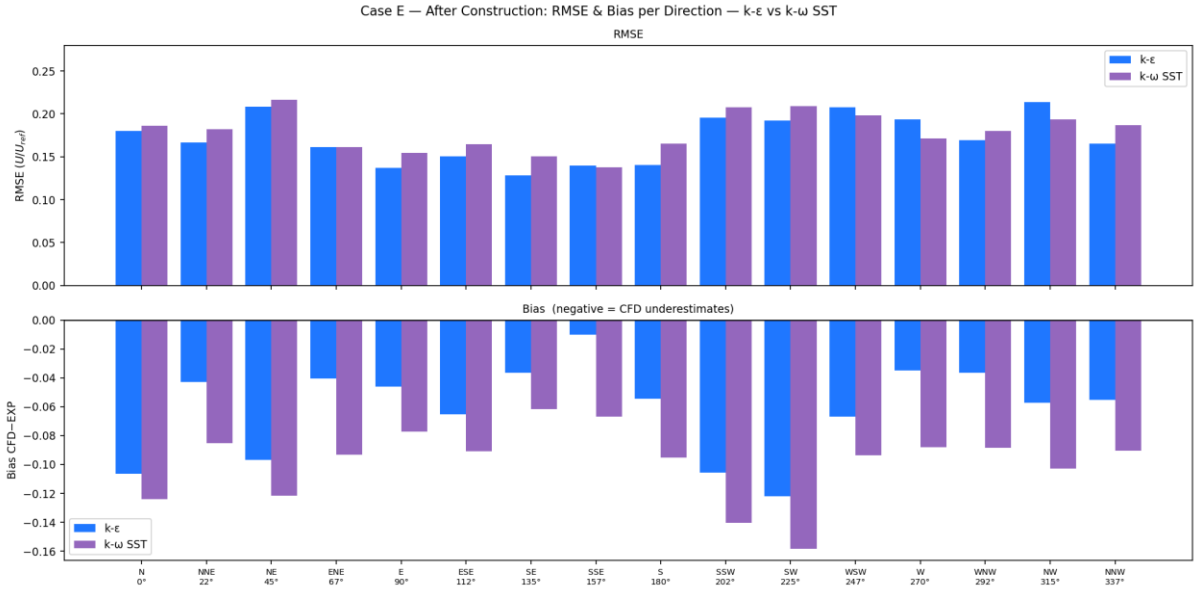


FIGURE 32 - RMSE AND BIAS PER WIND DIRECTION: REALIZABLE K-E (BLUE) VS. K-Ω SST (PURPLE).

3.6.3 ERROR DISTRIBUTION

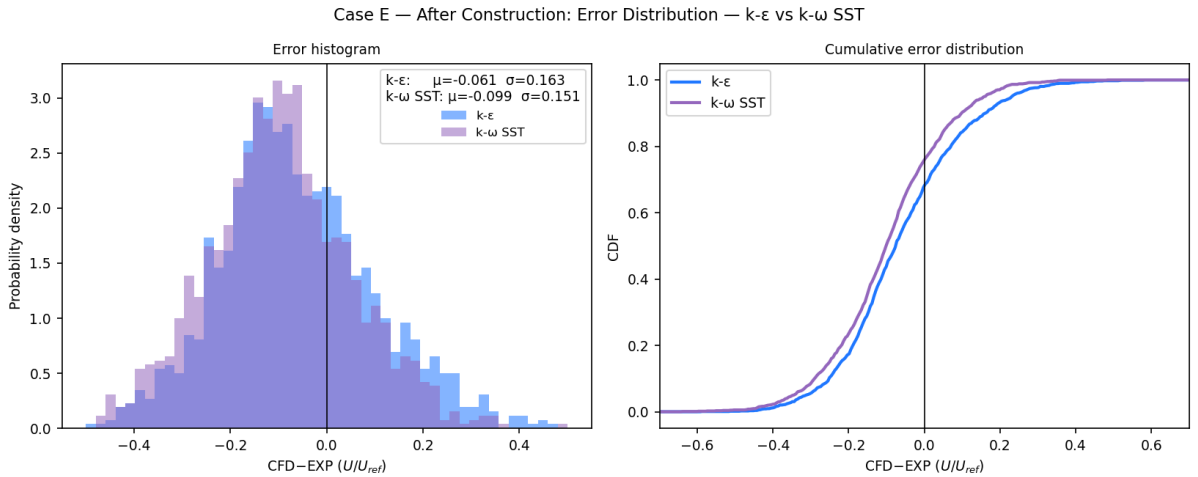


FIGURE 33 - ERROR DISTRIBUTION (CFD – EXP) —REALIZABLE K-E (BLUE) VS. K-Ω SST (PURPLE). LEFT: HISTOGRAM. RIGHT: CUMULATIVE DISTRIBUTION.

3.7 CONCLUSIONS

This validation study evaluated ArchiWind against AIJ Benchmark Case E, a dense urban environment with 80 probe points, 16 wind directions, and paired before/after construction datasets. The following conclusions are drawn:

Global accuracy is consistent across both configurations. After construction (k-ε): RMSE = 0.174, r = 0.769. Before construction: RMSE = 0.156, r = 0.603. These values are in line with the range reported in the literature for steady-state RANS simulations of complex urban wind fields [1, 2, 6].

ArchiWind correctly detects the wind impact of new construction. The spatial pattern and magnitude of ΔU (After − Before) match the wind tunnel measurements, confirming the solver's suitability for construction impact assessments.

A systematic negative bias is present (CFD underestimates wind speed), consistent with the known tendency of steady-state RANS to underpredict the extent of wake recovery in complex urban geometries. This bias is conservative for wind comfort assessments.

Draft mesh quality provides a reasonable approximation. Compared to Detailed: ΔRMSE = -0.002, Δr = 0.000. Draft results are suitable for rapid screening; Detailed is recommended for final assessments.

The k-ω SST turbulence model yields comparable global accuracy to Realizable k-ε (RMSE = 0.180, r = 0.771). Per-direction results show similar trends, with local differences at specific wind directions. Both models are suitable for pedestrian wind assessments.

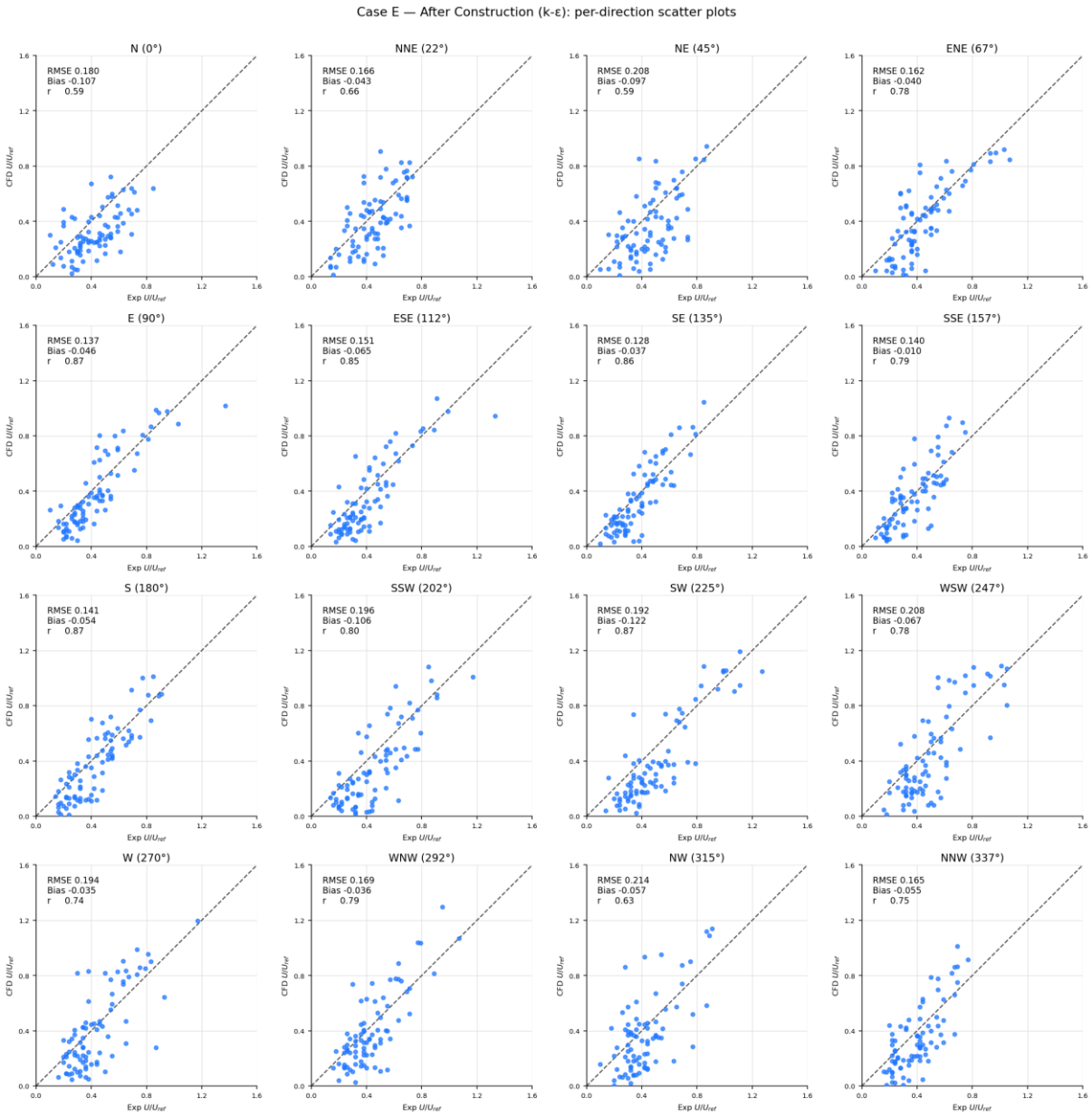
These results validate ArchiWind for pedestrian-level wind speed prediction in urban environments and support the use of the Realizable k-ε turbulence model as the default solver configuration

APPENDIX A — AFTER-CONSTRUCTION (REALIZABLE K- ε): ALL 16 WIND DIRECTIONS

Line plots for all 16 wind directions, After-Construction, Realizable k-ε model (Detailed mesh). Grey dashed: Experiment. Blue solid: ArchiWind.

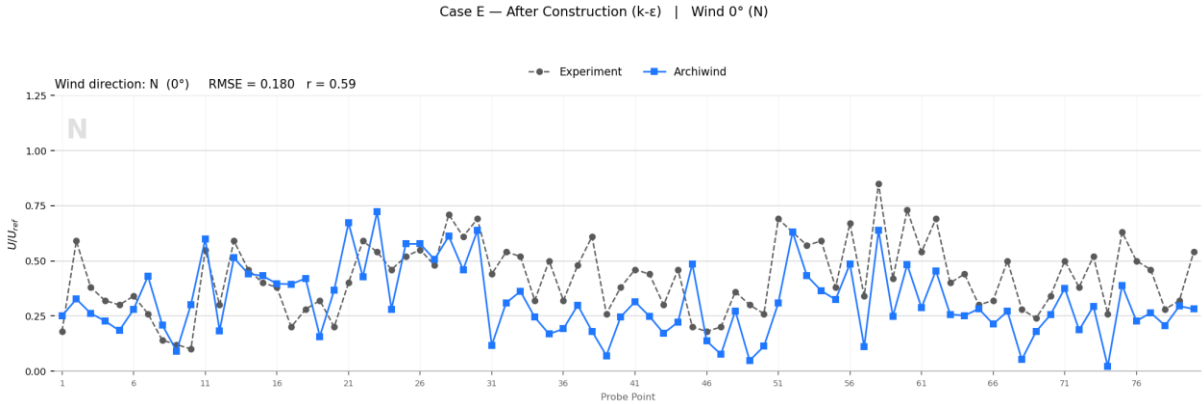
SCATTER PLOTS

Per-direction scatter plots of U/Uref: CFD vs Experiment. After-Construction (Realizable k-ε). RMSE, Bias and r values are shown in each plot.

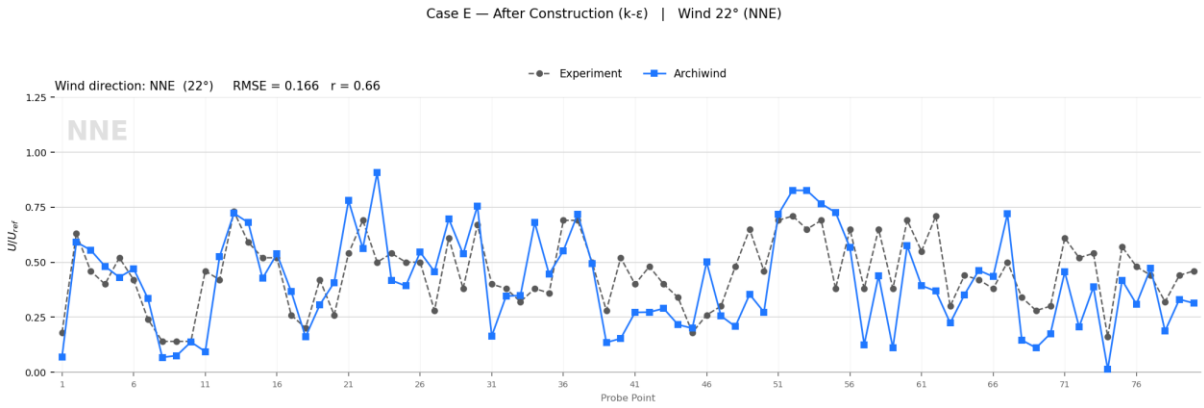


Per-direction scatter plots of U/Uref: CFD vs Experiment. After Construction (Realizable k-ε).

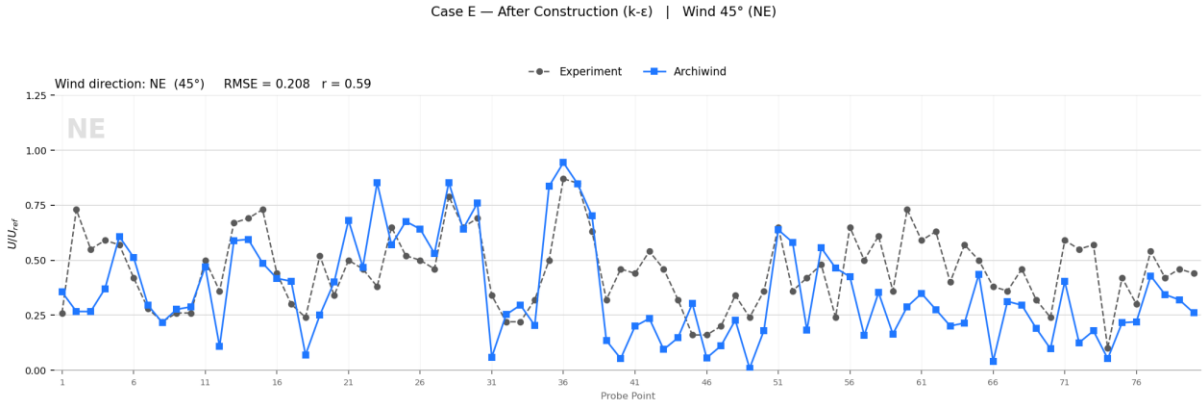
Experiment (grey dashed) vs. Archiwind (blue solid) for all 16 wind directions.



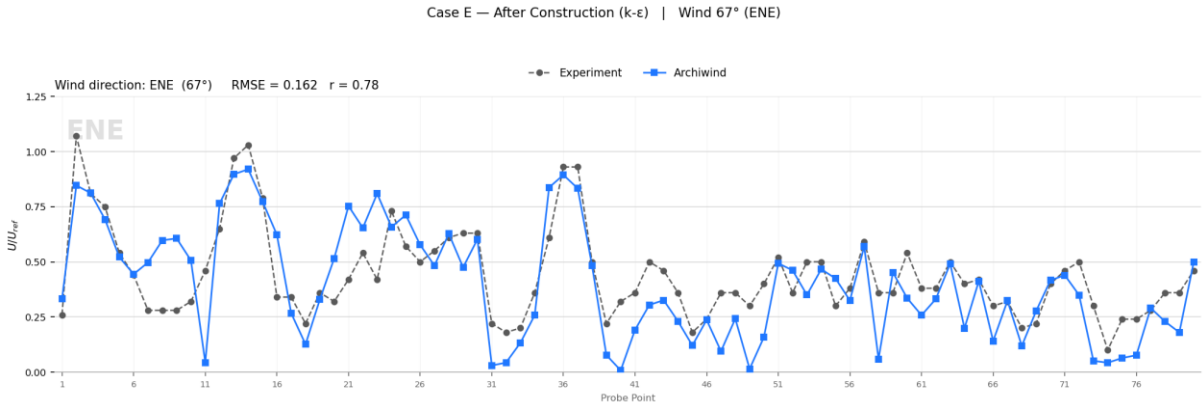
After Construction (k-ε) — Wind 0° (N). RMSE = 0.180 r = 0.589



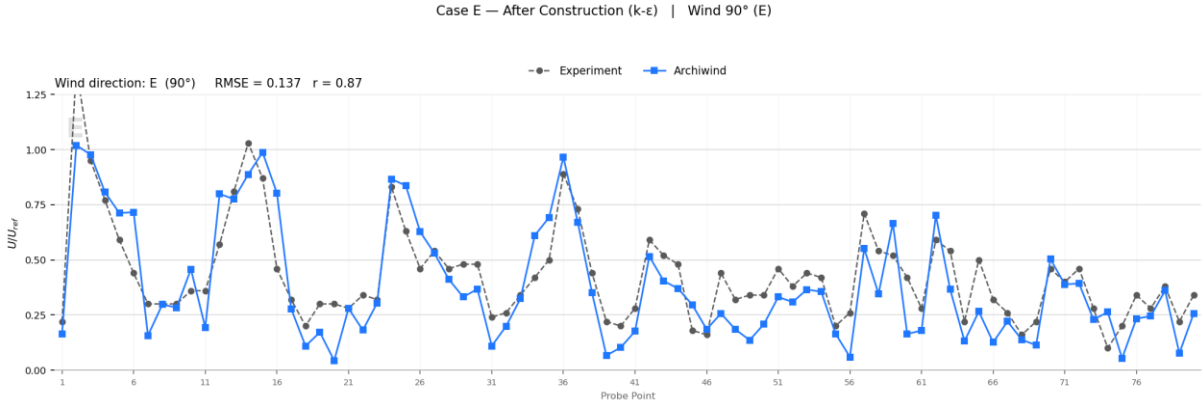
After Construction (k-ε) — Wind 22° (NNE). RMSE = 0.166 r = 0.664



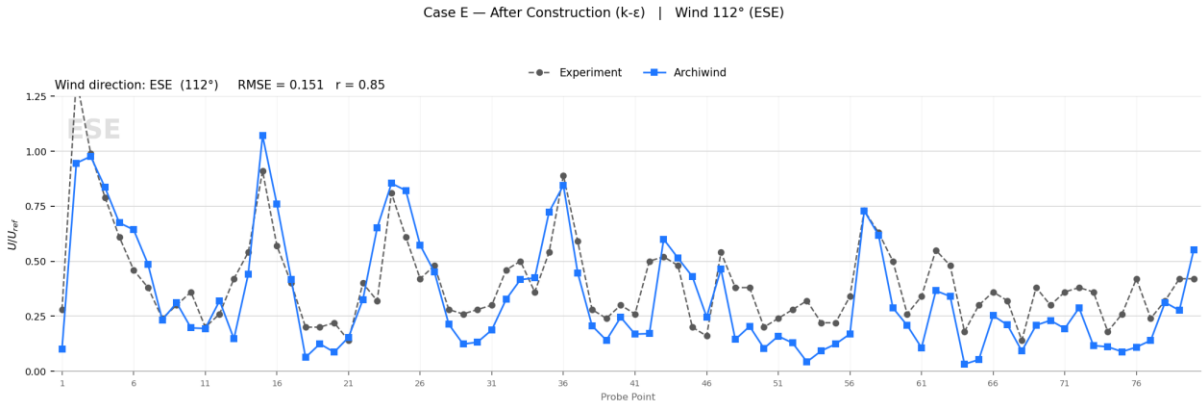
After Construction (k-ε) — Wind 45° (NE). RMSE = 0.208 r = 0.592



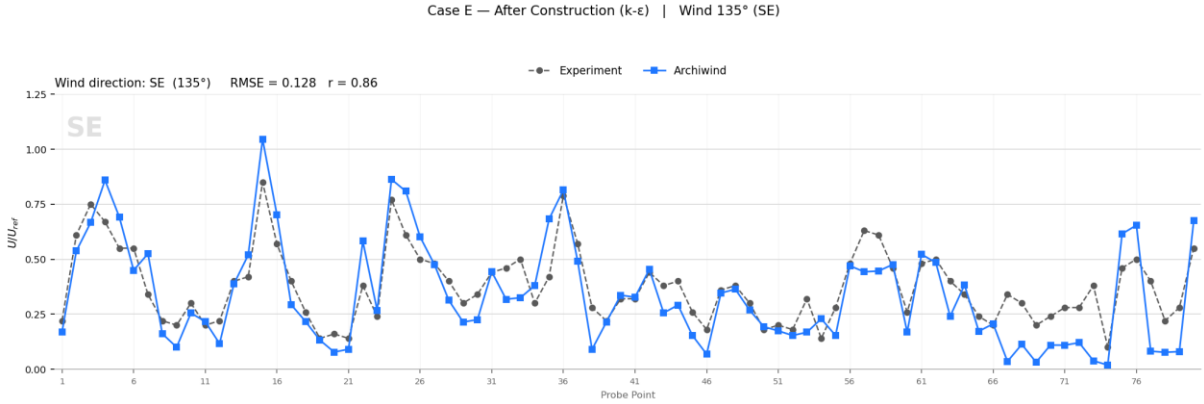
After Construction (k-ε) — Wind 67° (ENE). RMSE = 0.162 r = 0.784



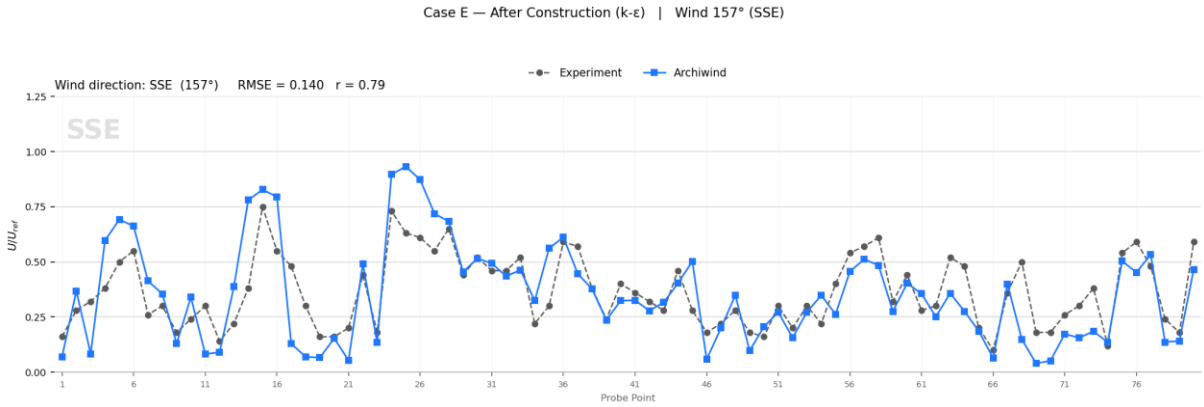
After Construction (k-ε) — Wind 90° (E). RMSE = 0.137 r = 0.869



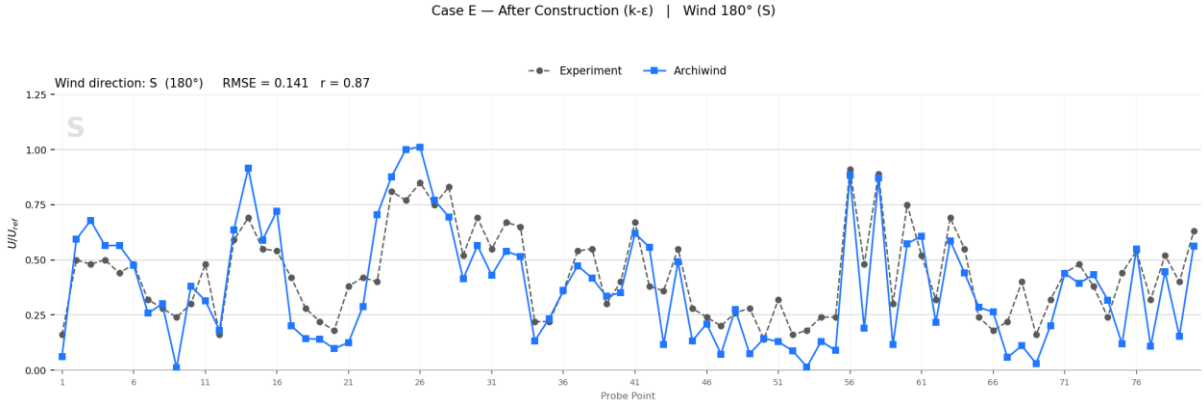
After Construction (k-ε) — Wind 112° (ESE). RMSE = 0.151 r = 0.845



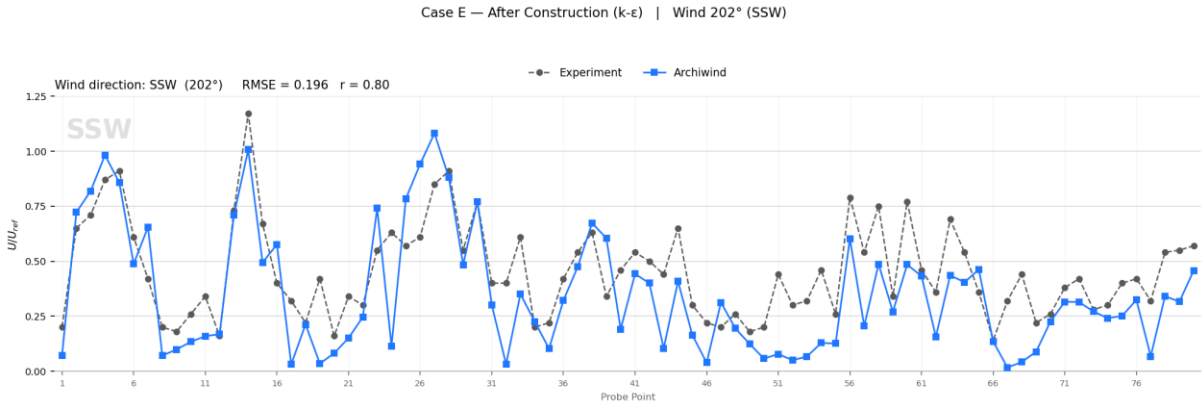
After Construction (k-ε) — Wind 135° (SE). RMSE = 0.128 r = 0.864



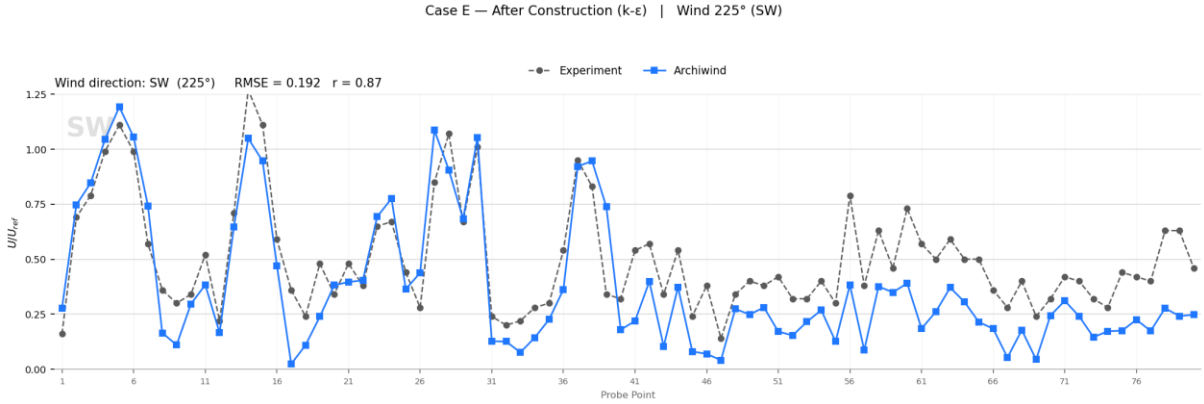
After Construction (k-ε) — Wind 157° (SSE). RMSE = 0.140 r = 0.787



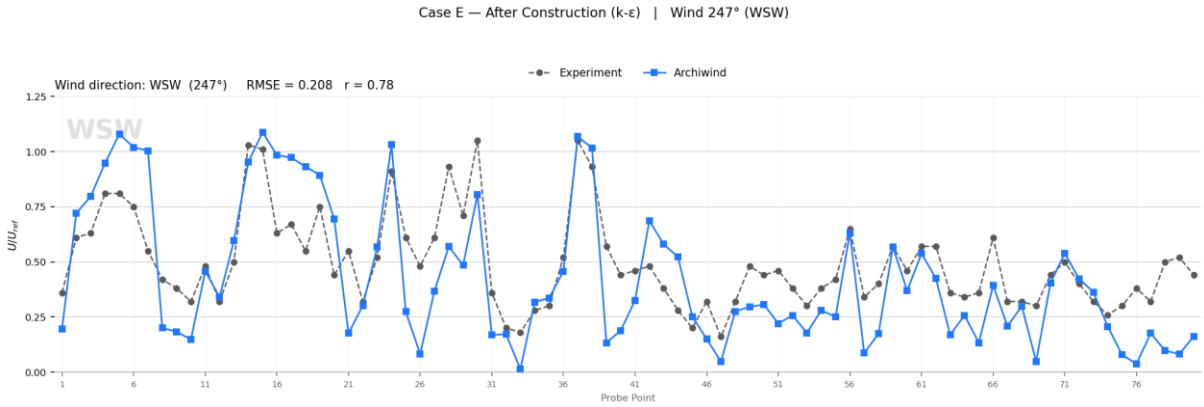
After Construction (k-ε) — Wind 180° (S). RMSE = 0.141 r = 0.867



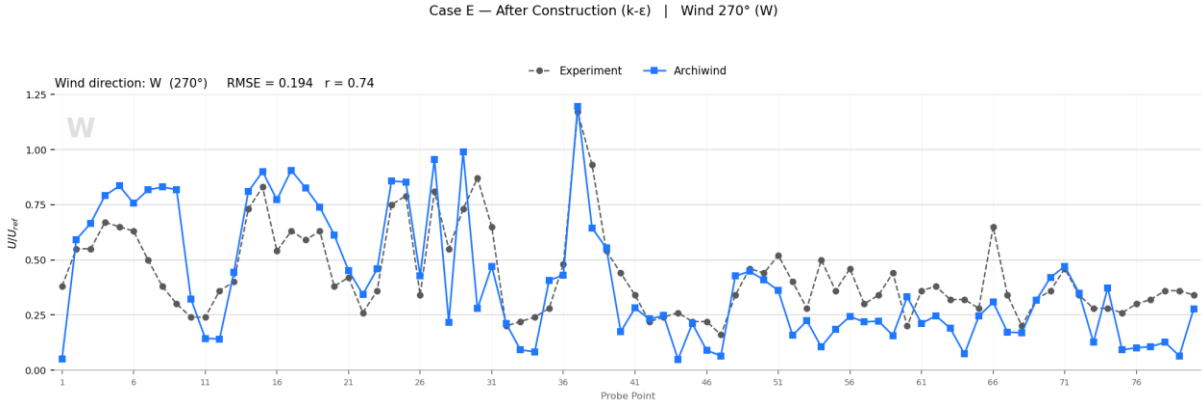
After Construction (k-ε) — Wind 202° (SSW). RMSE = 0.196 r = 0.798



After Construction (k-ε) — Wind 225° (SW). RMSE = 0.192 r = 0.874



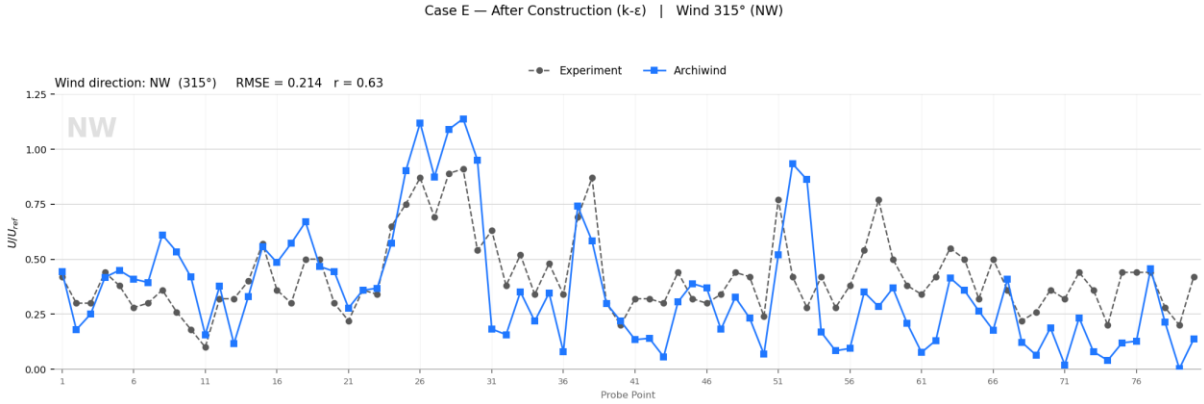
After Construction (k-ε) — Wind 247° (WSW). RMSE = 0.208 r = 0.780



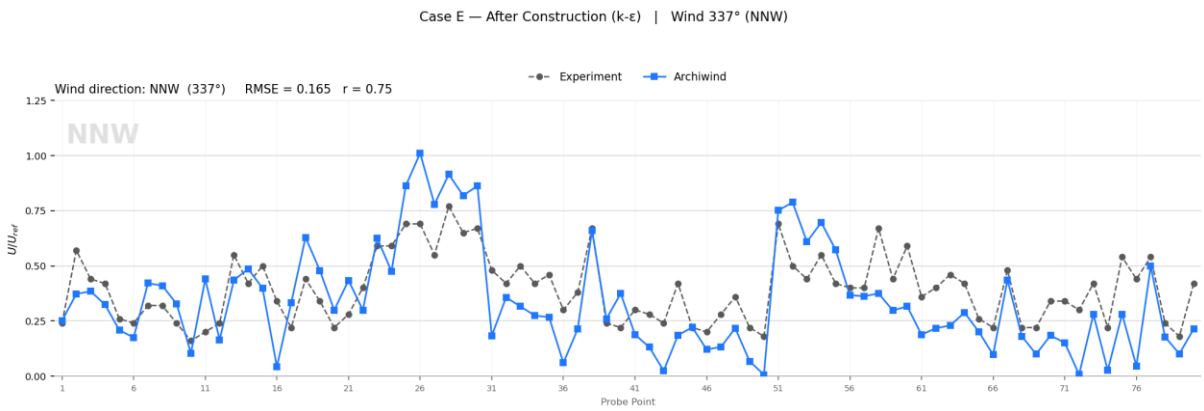
After Construction (k-ε) — Wind 270° (W). RMSE = 0.194 r = 0.739



After Construction (k-ε) — Wind 292° (WNW). RMSE = 0.169 r = 0.789



After Construction (k-ε) — Wind 315° (NW). RMSE = 0.214 r = 0.635



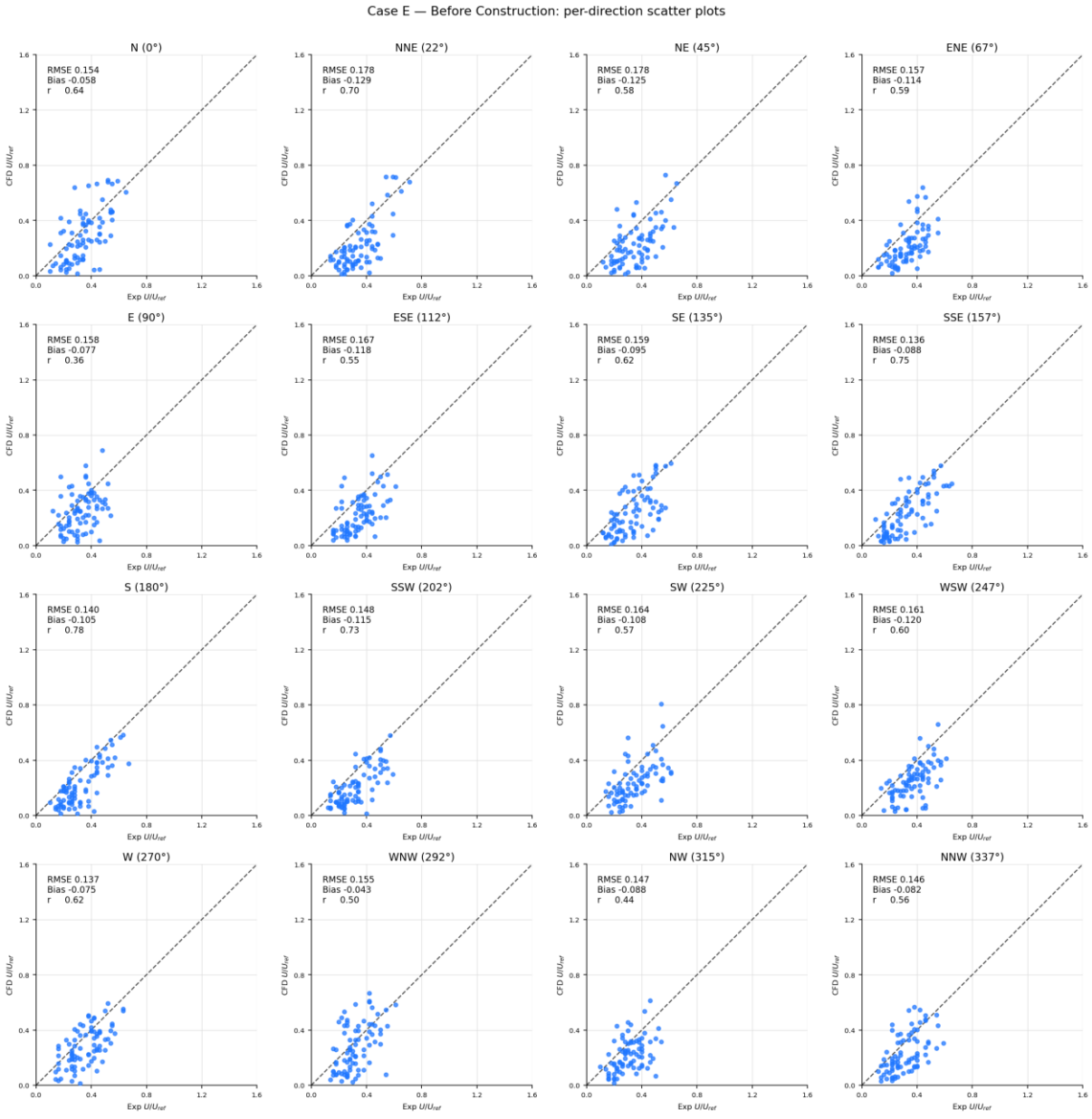
After Construction (k-ε) — Wind 337° (NNW). RMSE = 0.165 r = 0.748

APPENDIX B — BEFORE-CONSTRUCTION: ALL 16 WIND DIRECTIONS

Line plots for all 16 wind directions, Before-Construction (Detailed mesh).

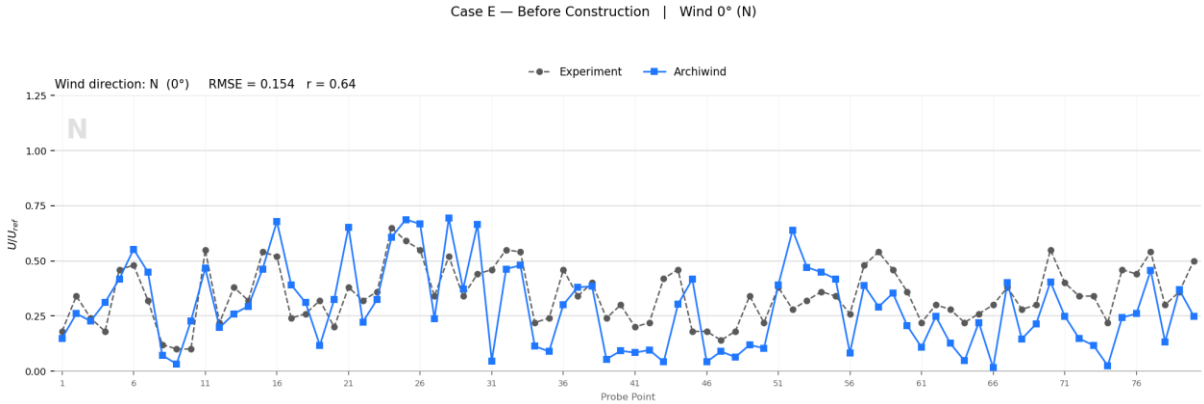
SCATTER PLOTS

Per-direction scatter plots of U/Uref: CFD vs Experiment. Before-Construction. RMSE, Bias and r values are shown in each plot.

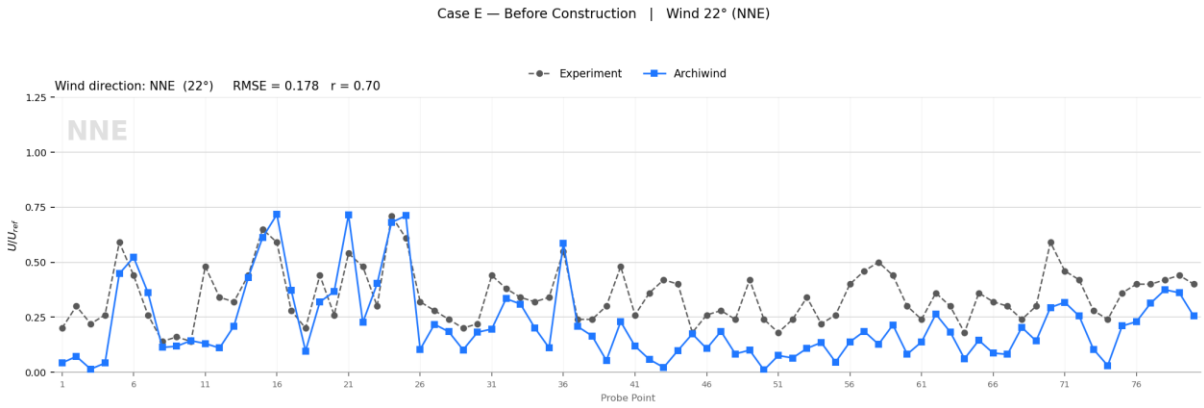


Per-direction scatter plots of U/Uref: CFD vs Experiment. Before Construction.

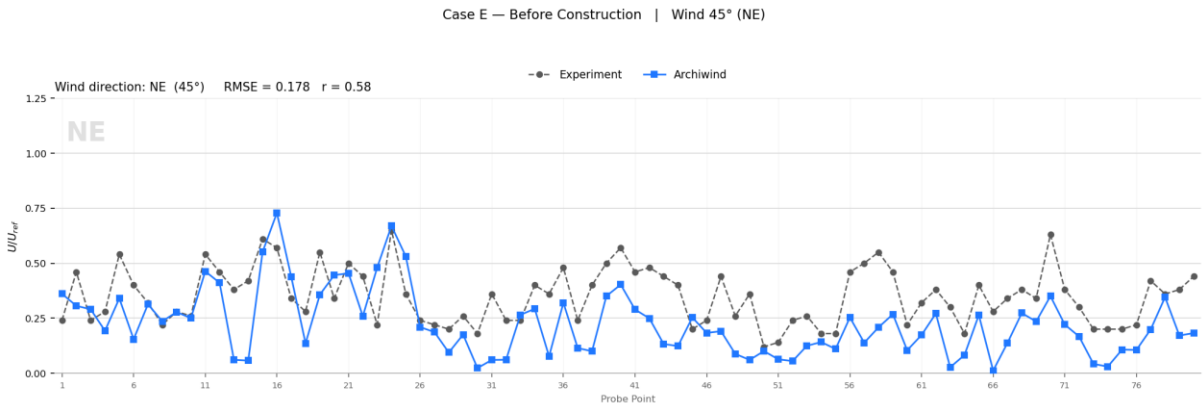
Experiment (grey dashed) vs. Archiwind (blue solid) for all 16 wind directions.



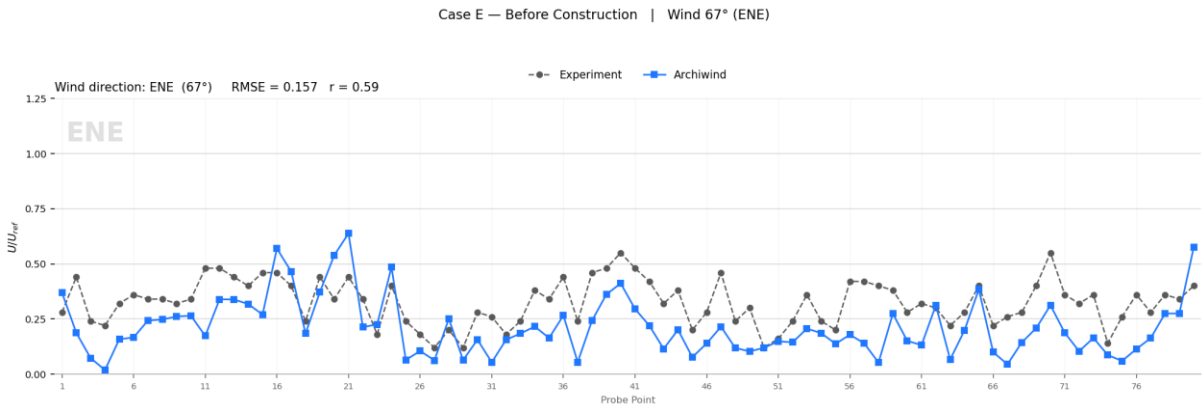
Before Construction — Wind 0° (N). RMSE = 0.154 r = 0.640



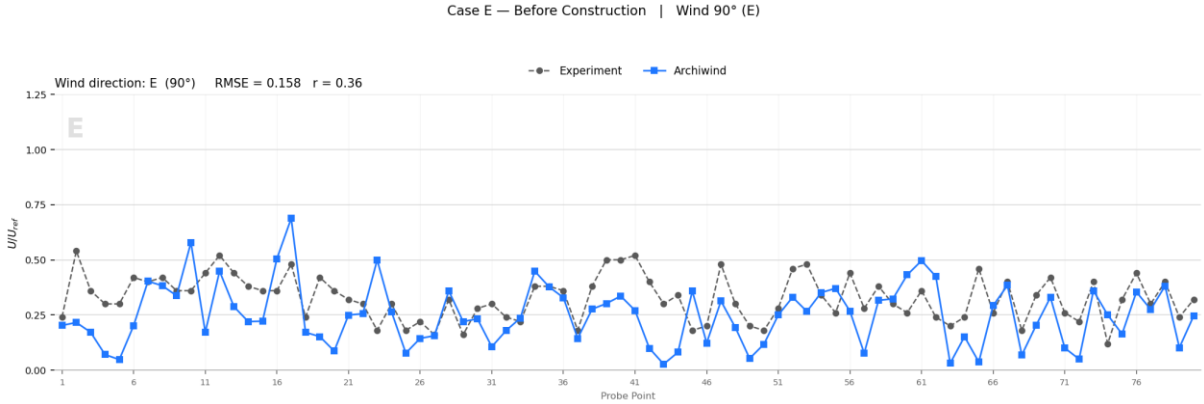
Before Construction — Wind 22° (NNE). RMSE = 0.178 r = 0.699



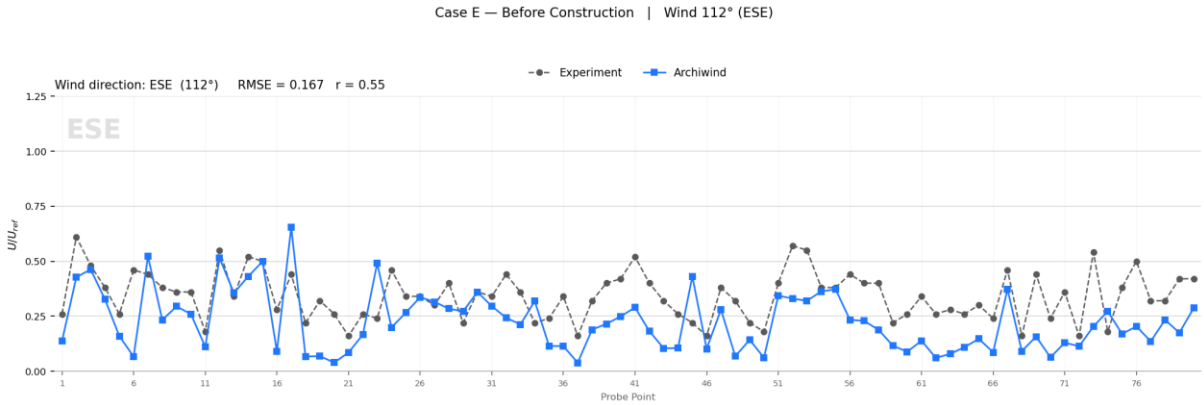
Before Construction — Wind 45° (NE). RMSE = 0.178 r = 0.584



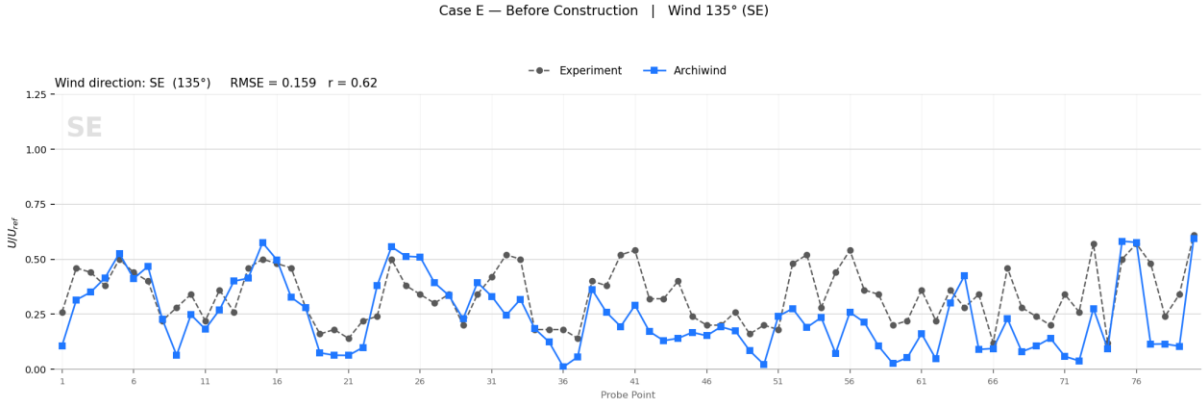
Before Construction — Wind 67° (ENE). RMSE = 0.157 r = 0.592



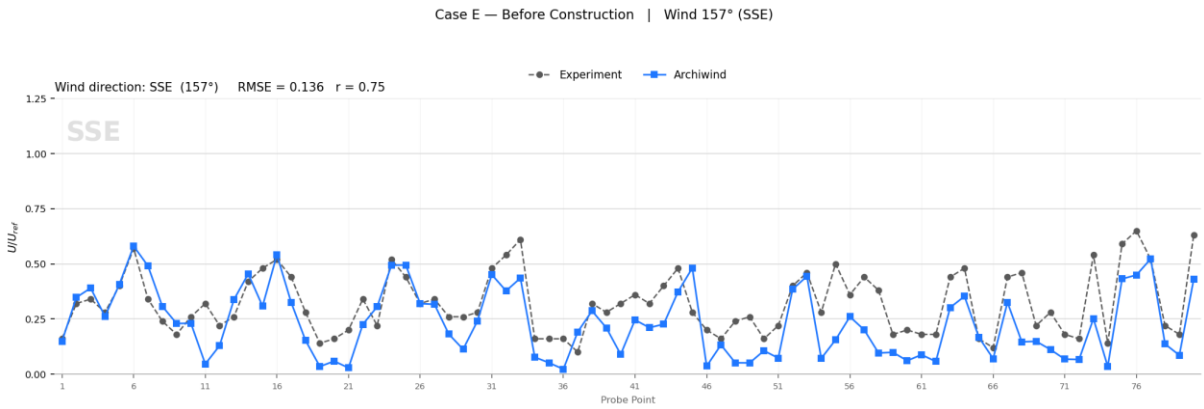
Before Construction — Wind 90° (E). RMSE = 0.158 r = 0.364



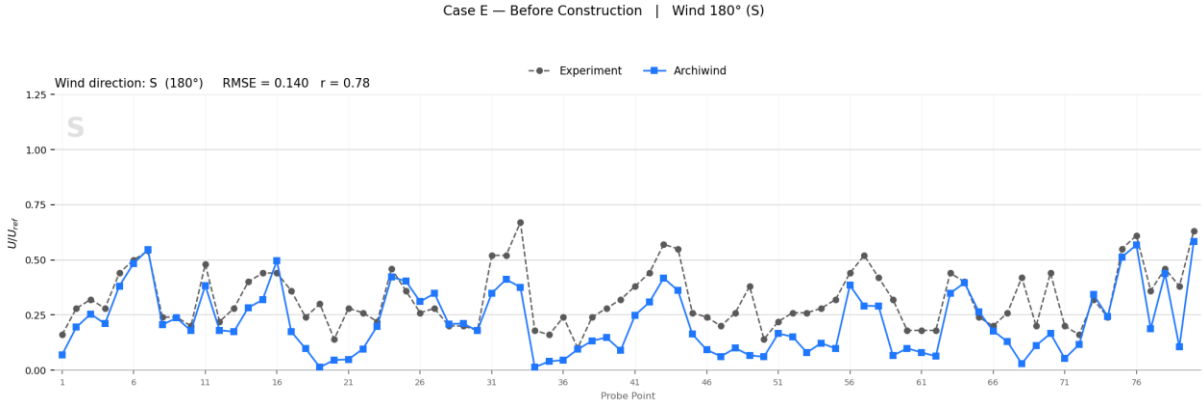
Before Construction — Wind 112° (ESE). RMSE = 0.167 r = 0.549



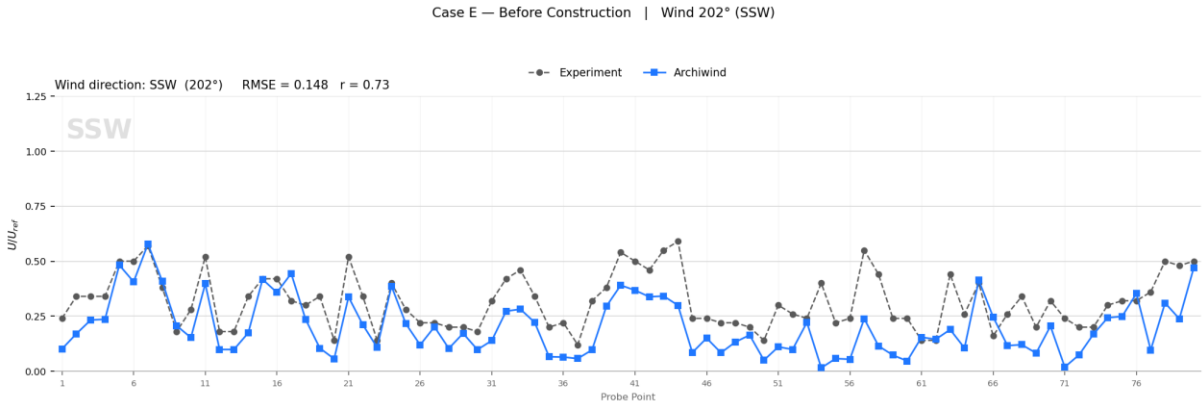
Before Construction — Wind 135° (SE). RMSE = 0.159 r = 0.623



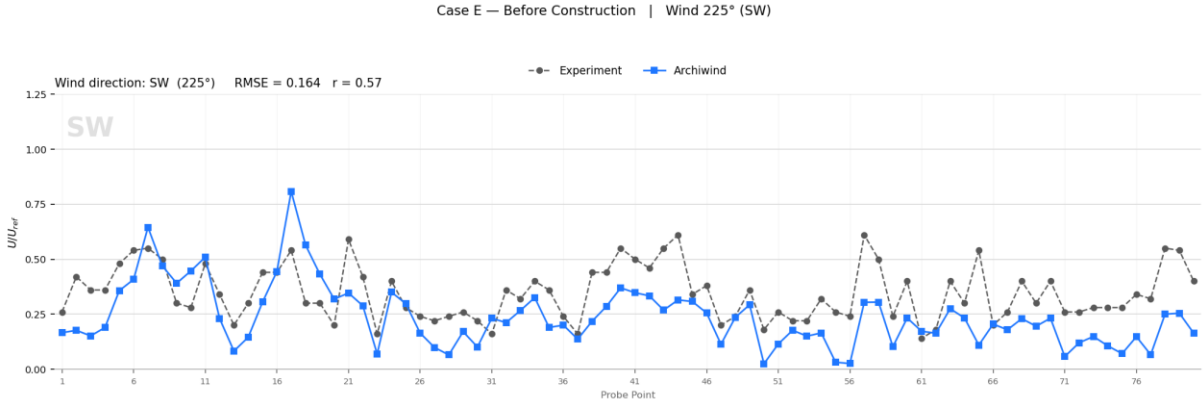
Before Construction — Wind 157° (SSE). RMSE = 0.136 r = 0.755



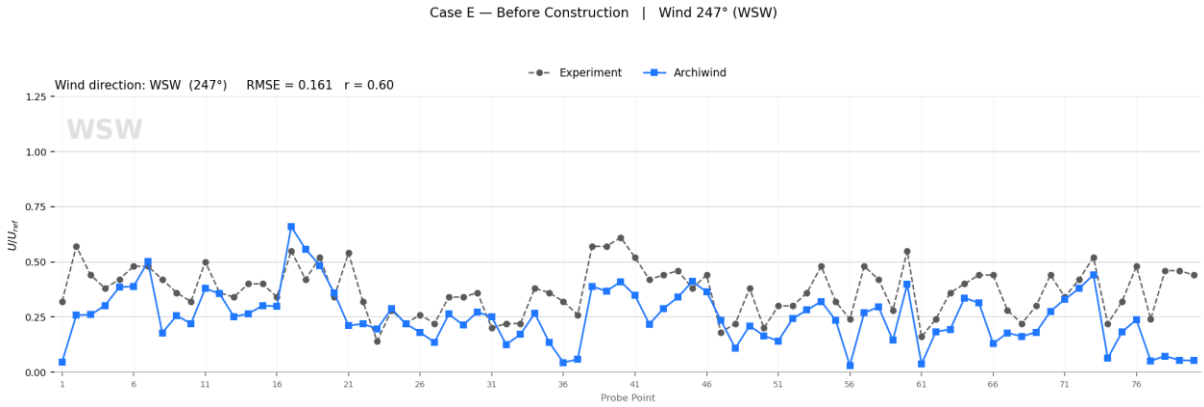
Before Construction — Wind 180° (S). RMSE = 0.140 r = 0.780



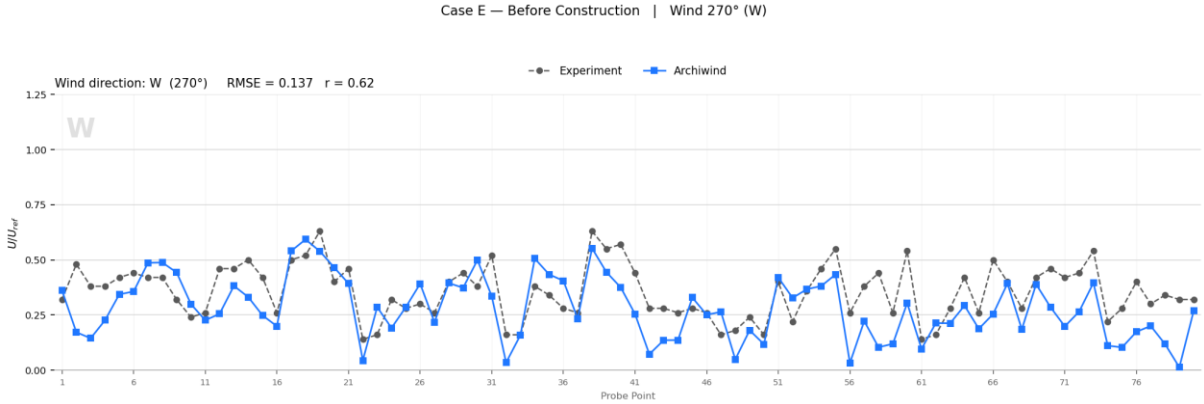
Before Construction — Wind 202° (SSW). RMSE = 0.148 r = 0.727



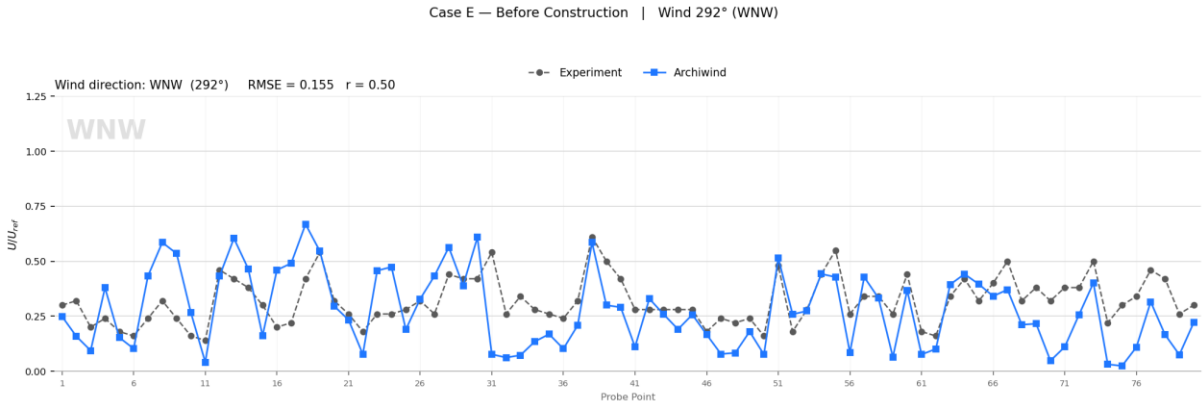
Before Construction — Wind 225° (SW). RMSE = 0.164 r = 0.573



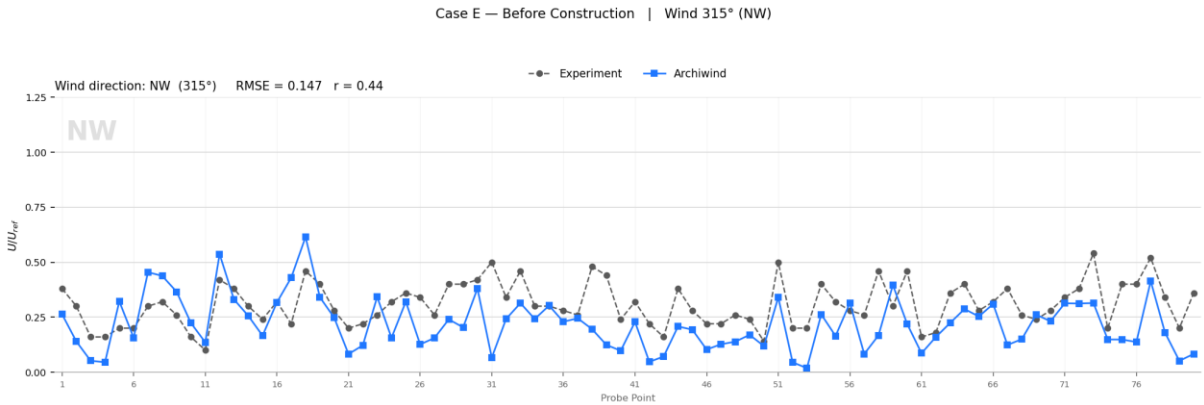
Before Construction — Wind 247° (WSW). RMSE = 0.161 r = 0.599



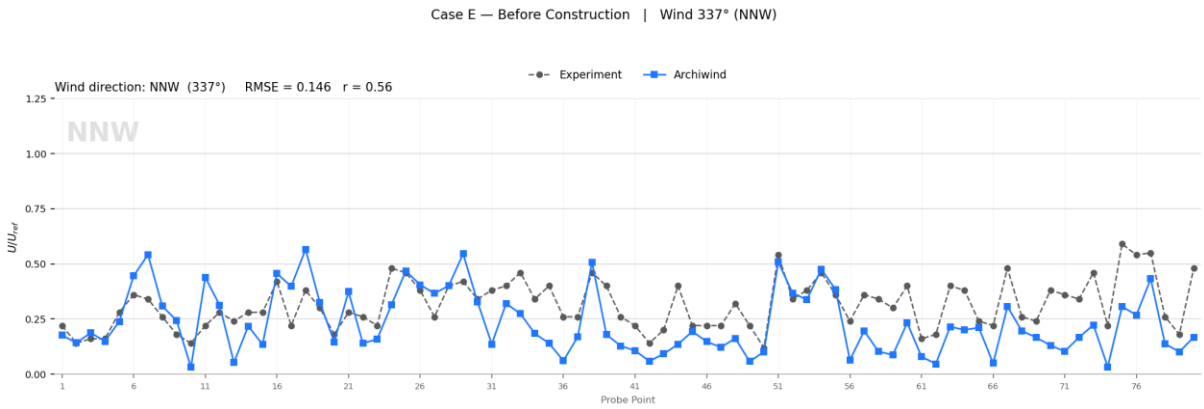
Before Construction — Wind 270° (W). RMSE = 0.137 r = 0.620



Before Construction — Wind 292° (WNW). RMSE = 0.155 r = 0.504



Before Construction — Wind 315° (NW). RMSE = 0.147 r = 0.442



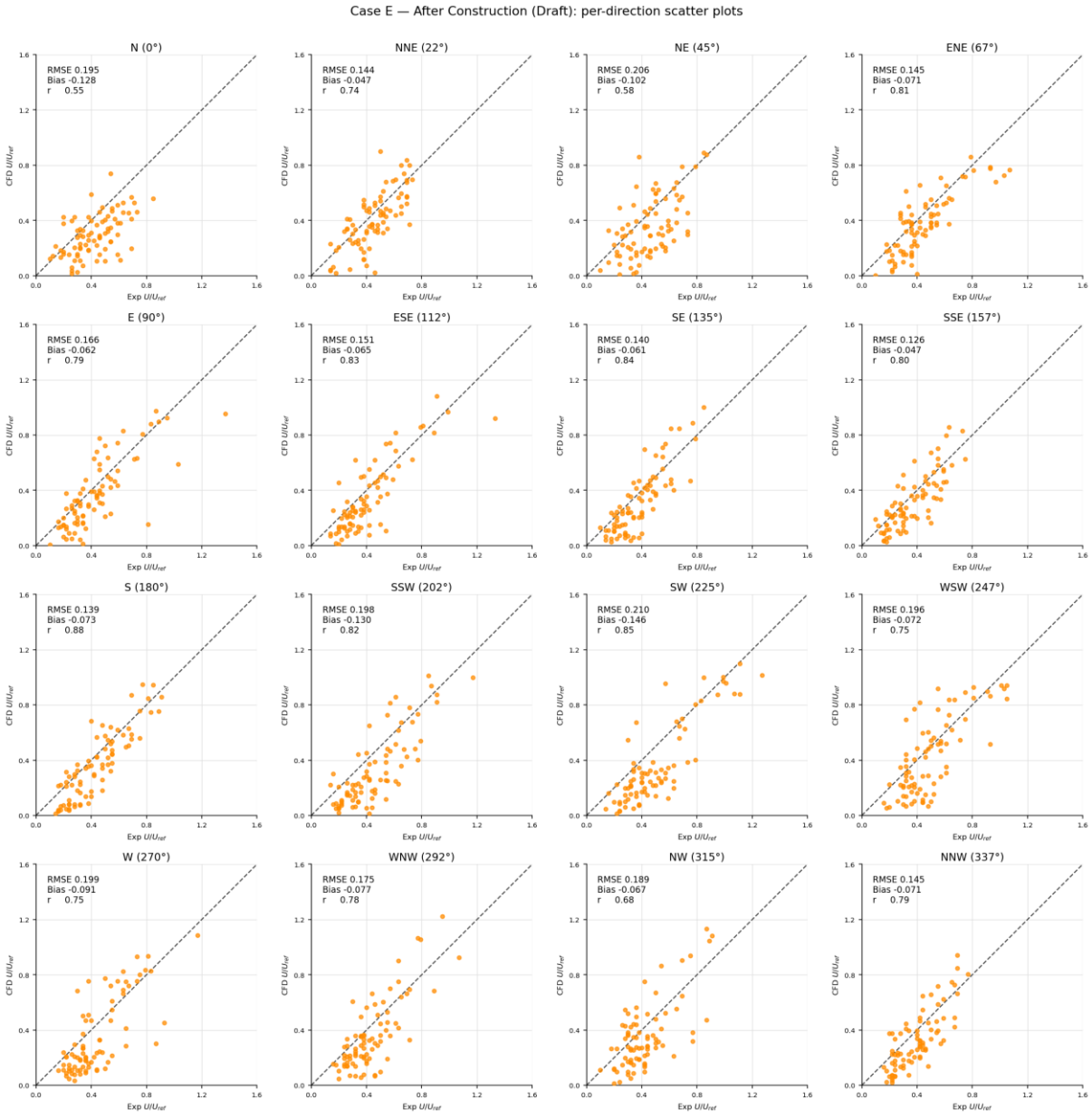
Before Construction — Wind 337° (NNW). RMSE = 0.146 r = 0.560

APPENDIX C — AFTER-CONSTRUCTION (DRAFT): ALL 16 WIND DIRECTIONS

Line plots for all 16 wind directions, After-Construction (Draft mesh quality).

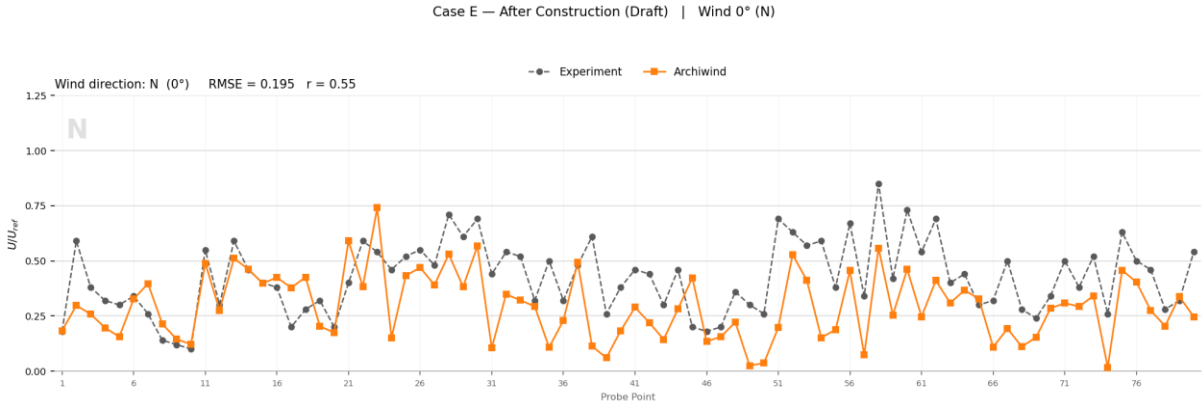
SCATTER PLOTS

Per-direction scatter plots of U/Uref: CFD vs Experiment. After-Construction (Draft). RMSE, Bias and r values are shown in each plot.

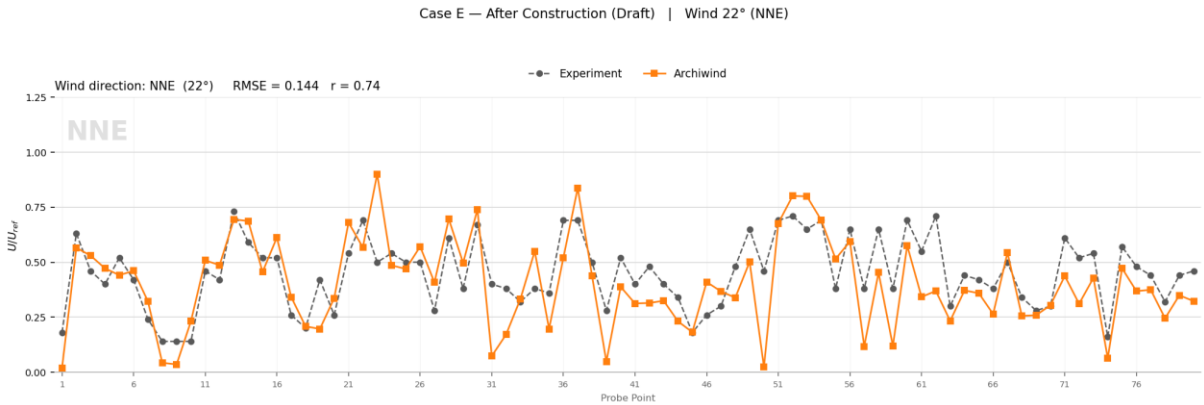


Per-direction scatter plots of U/Uref: CFD vs Experiment. After Construction (Draft).

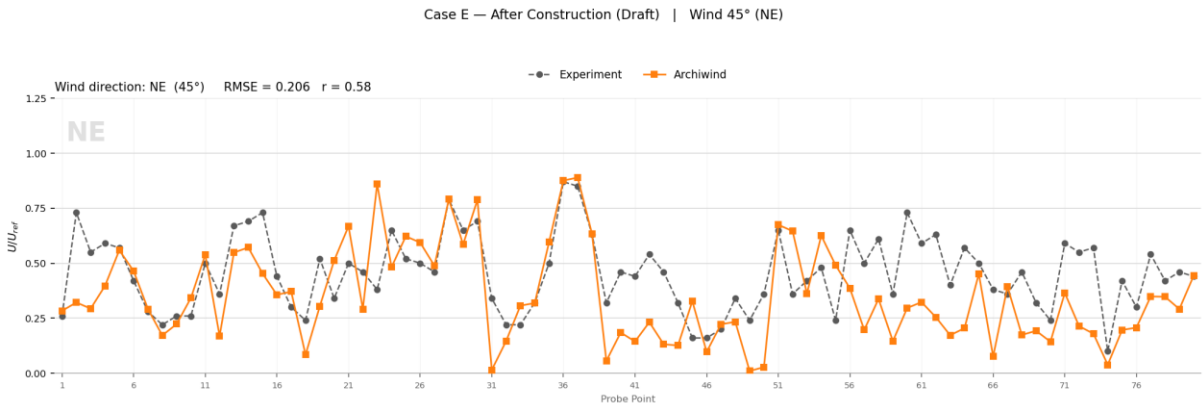
Experiment (grey dashed) vs. Archiwind (orange solid) for all 16 wind directions.



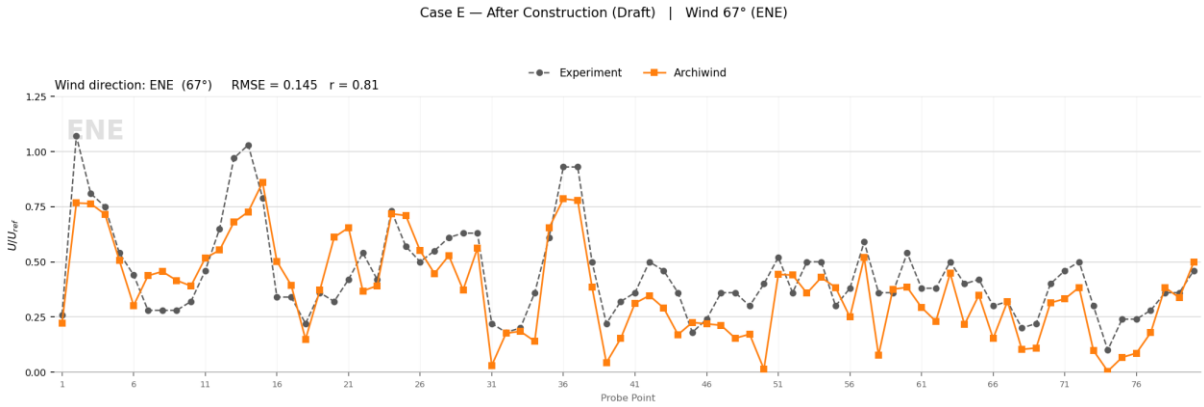
After Construction (Draft) — Wind 0° (N). RMSE = 0.195 r = 0.549



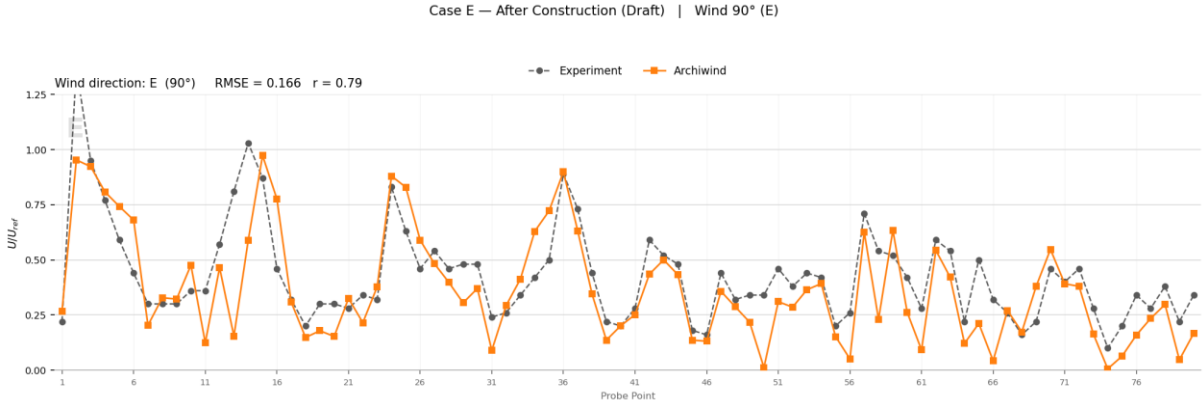
After Construction (Draft) — Wind 22° (NNE). RMSE = 0.144 r = 0.738



After Construction (Draft) — Wind 45° (NE). RMSE = 0.206 r = 0.582



After Construction (Draft) — Wind 67° (ENE). RMSE = 0.145 r = 0.814



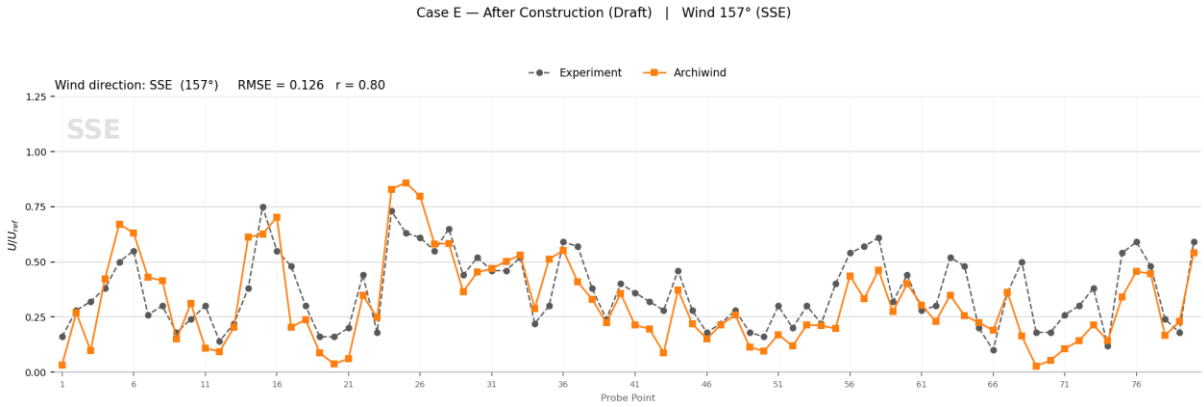
After Construction (Draft) — Wind 90° (E). RMSE = 0.166 r = 0.785



After Construction (Draft) — Wind 112° (ESE). RMSE = 0.151 r = 0.835



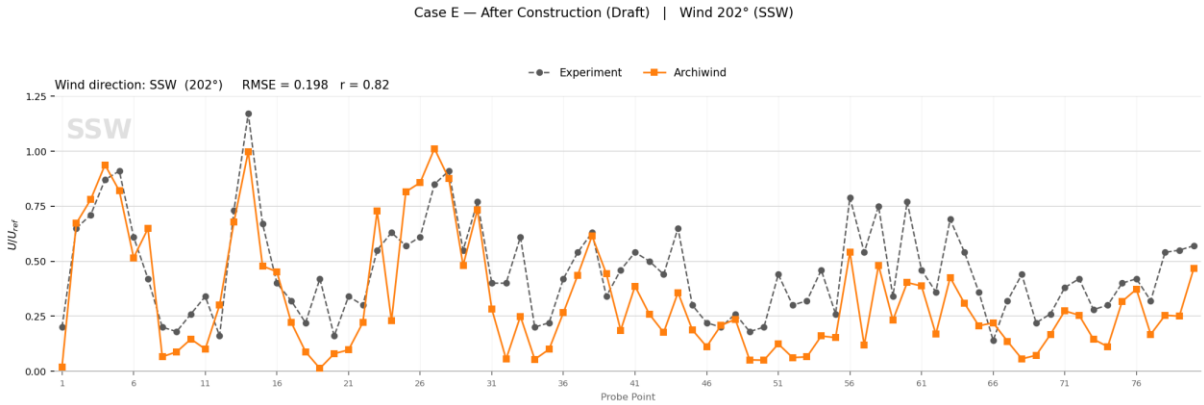
After Construction (Draft) — Wind 135° (SE). RMSE = 0.140 r = 0.839



After Construction (Draft) — Wind 157° (SSE). RMSE = 0.126 r = 0.803



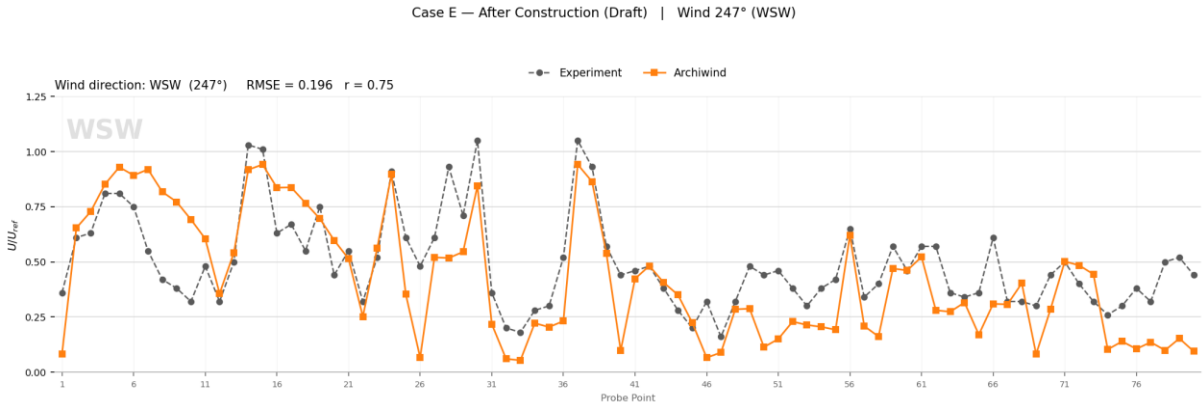
After Construction (Draft) — Wind 180° (S). RMSE = 0.139 r = 0.880



After Construction (Draft) — Wind 202° (SSW). RMSE = 0.198 r = 0.816



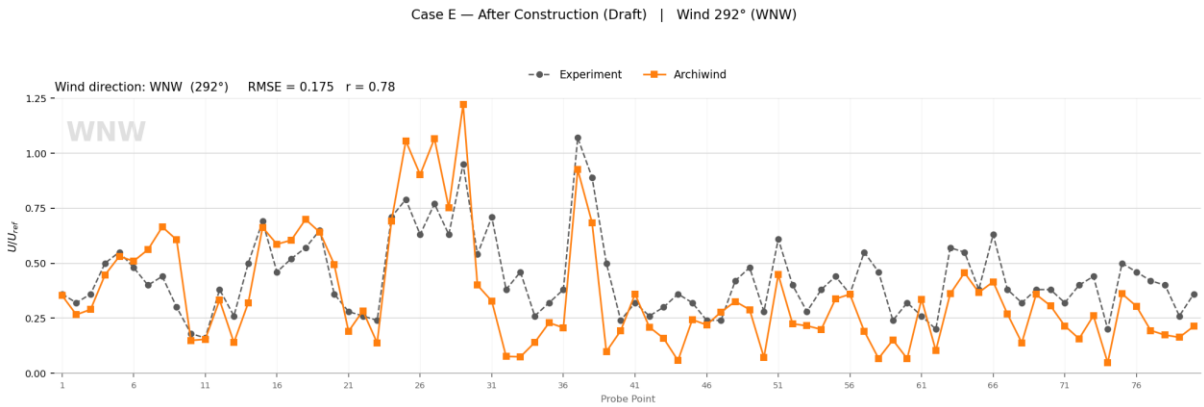
After Construction (Draft) — Wind 225° (SW). RMSE = 0.210 r = 0.852



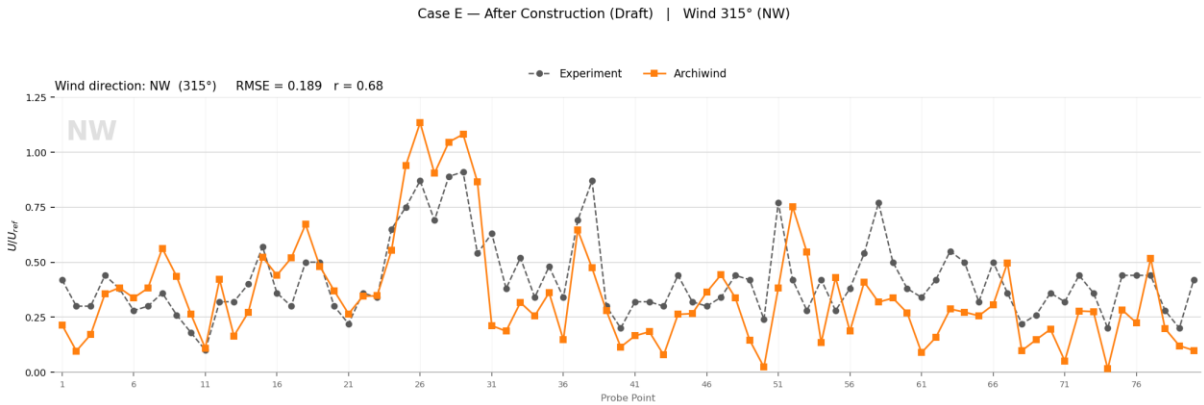
After Construction (Draft) — Wind 247° (WSW). RMSE = 0.196 r = 0.749



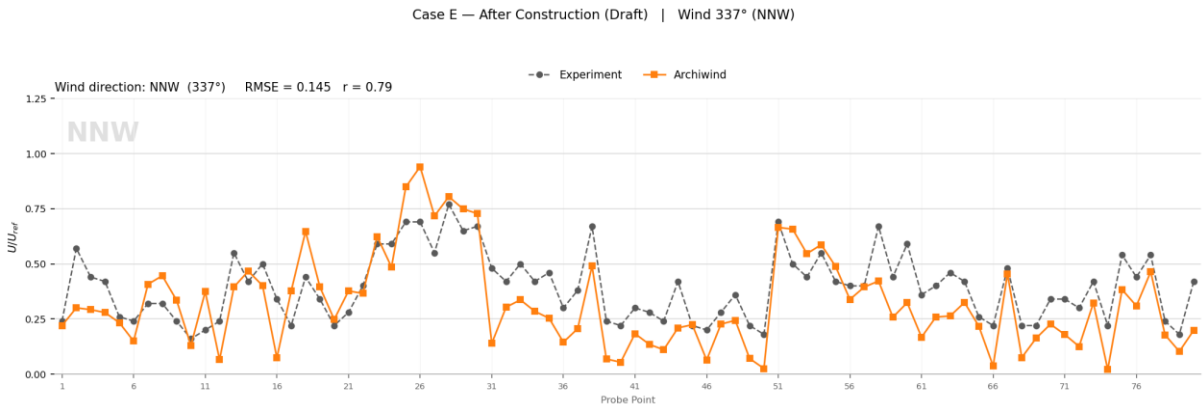
After Construction (Draft) — Wind 270° (W). RMSE = 0.199 r = 0.750



After Construction (Draft) — Wind 292° (WNW). RMSE = 0.175 r = 0.780



After Construction (Draft) — Wind 315° (NW). RMSE = 0.189 r = 0.679



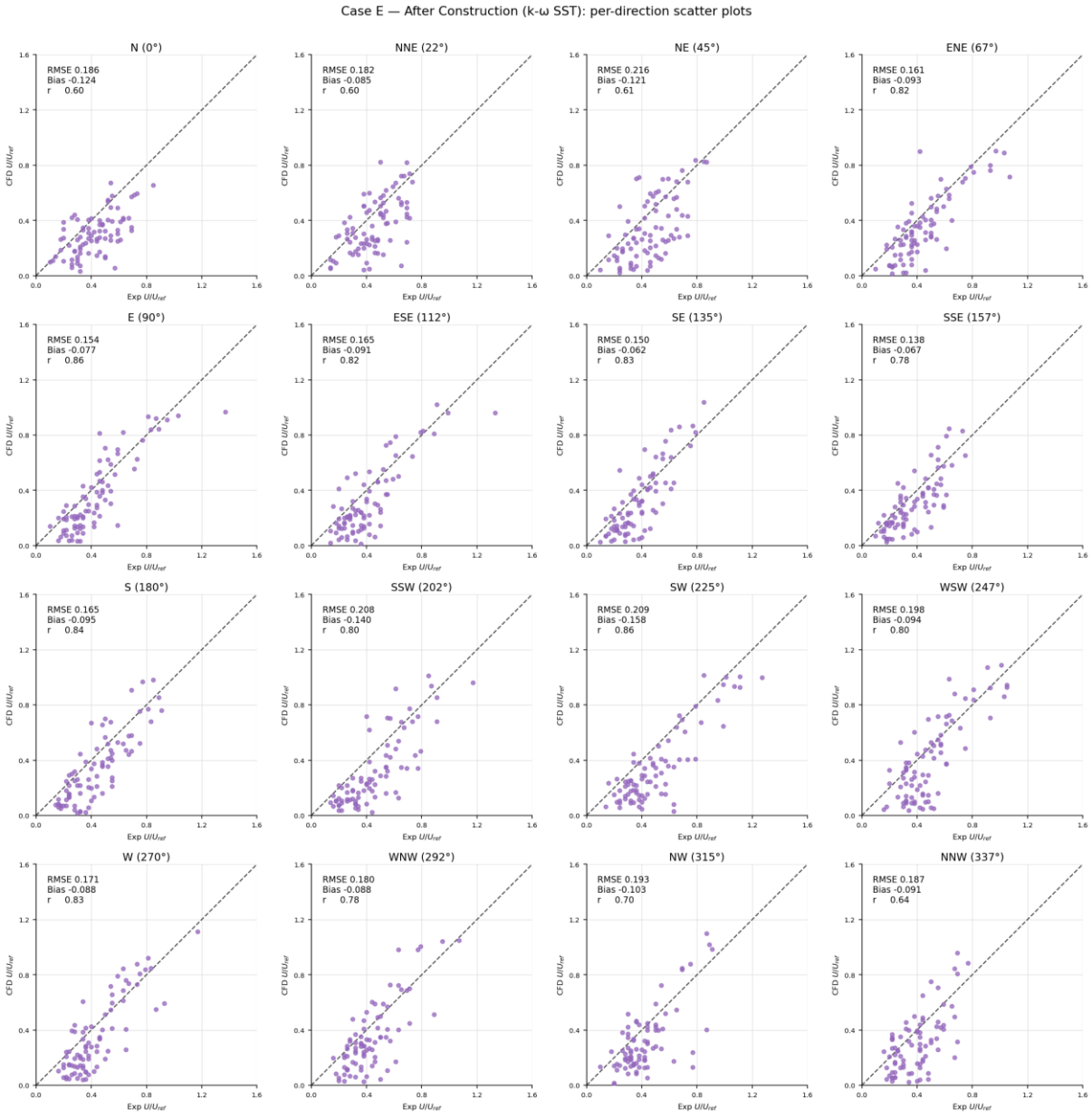
After Construction (Draft) — Wind 337° (NNW). RMSE = 0.145 r = 0.791

APPENDIX D — AFTER-CONSTRUCTION (K-Ω SST): ALL 16 WIND DIRECTIONS

Line plots for all 16 wind directions, After-Construction, k-ω SST model (Detailed mesh). Grey dashed: Experiment. Purple solid: ArchiWind (k-ω SST).

SCATTER PLOTS

Per-direction scatter plots of U/Uref: CFD vs Experiment. After-Construction (k-ω SST). RMSE, Bias and r values are shown in each plot.

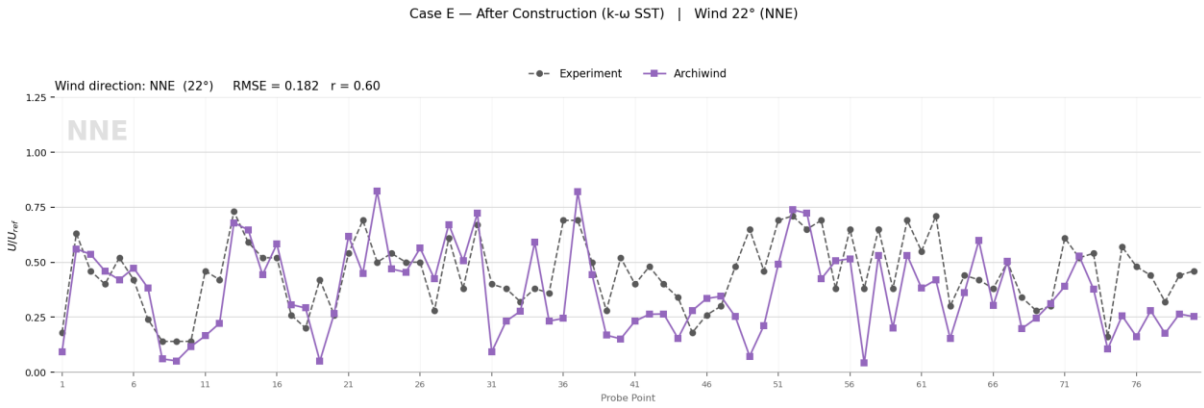


Per-direction scatter plots of U/Uref: CFD vs Experiment. After Construction (k-ω SST).

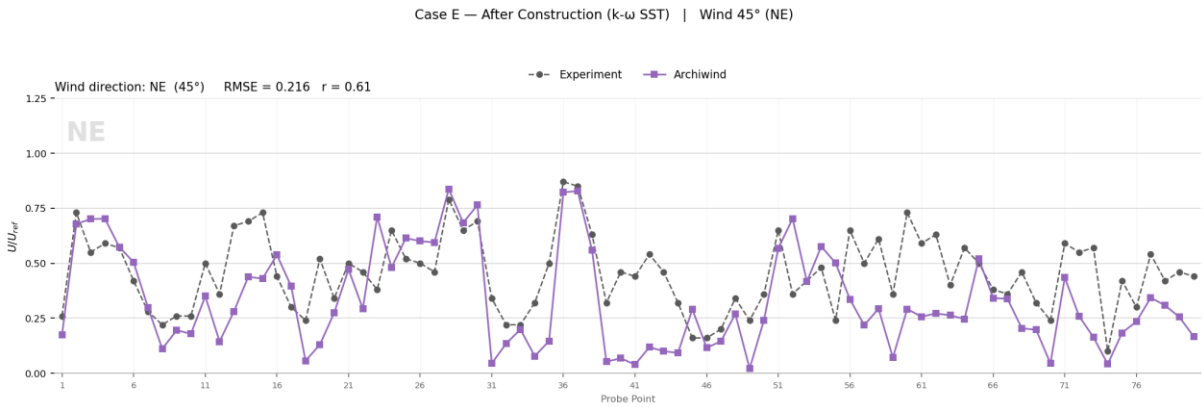
Experiment (grey dashed) vs. ArchiWind (purple solid) for all 16 wind directions.



After Construction (k-ω SST) — Wind 0° (N). RMSE = 0.186 r = 0.597



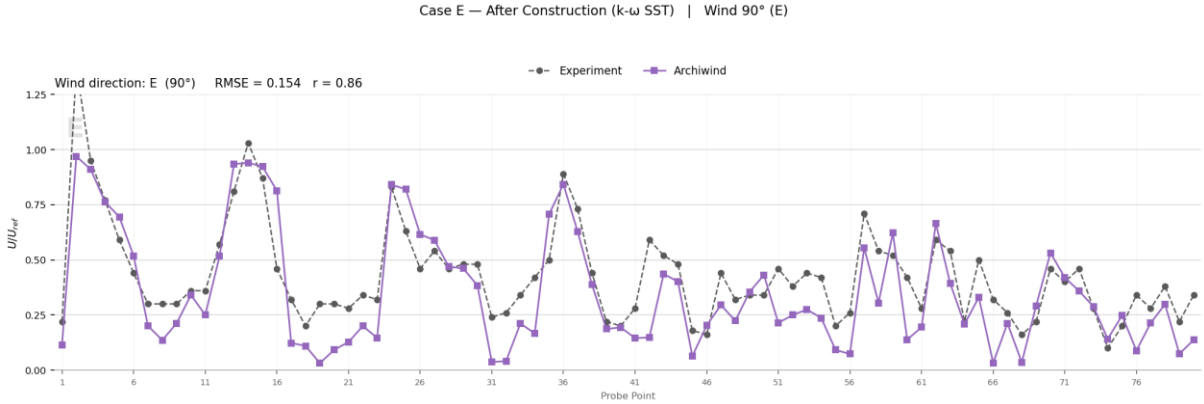
After Construction (k-ω SST) — Wind 22° (NNE). RMSE = 0.182 r = 0.596



After Construction (k-ω SST) — Wind 45° (NE). RMSE = 0.216 r = 0.607



After Construction (k-ω SST) — Wind 67° (ENE). RMSE = 0.161 r = 0.819



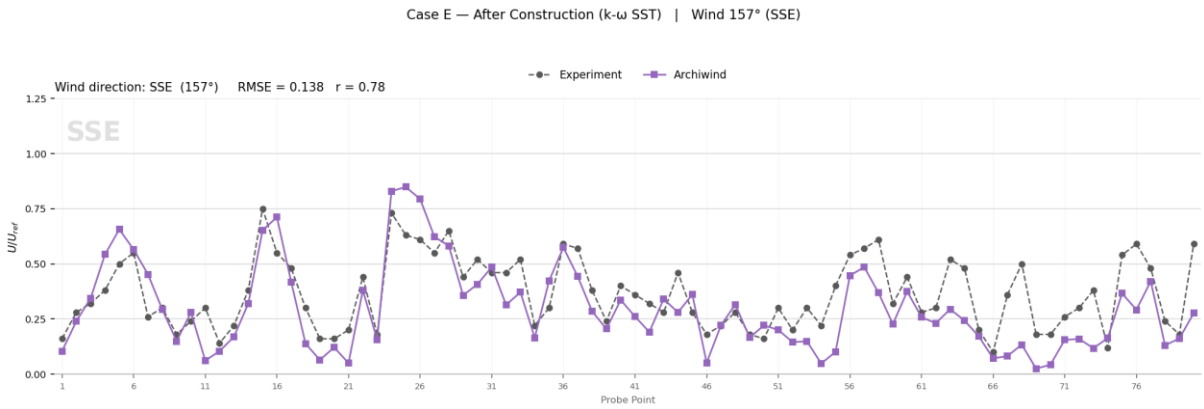
After Construction (k-ω SST) — Wind 90° (E). RMSE = 0.154 r = 0.859



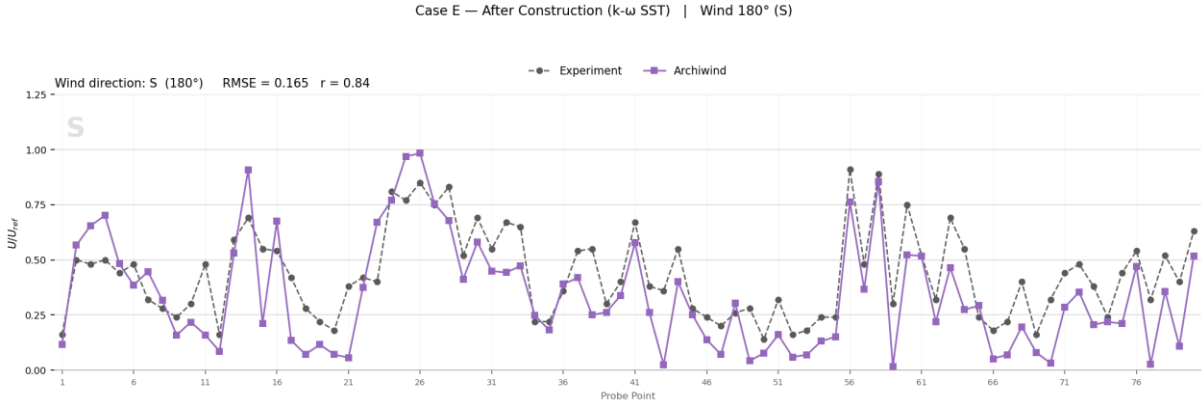
After Construction (k-ω SST) — Wind 112° (ESE). RMSE = 0.165 r = 0.825



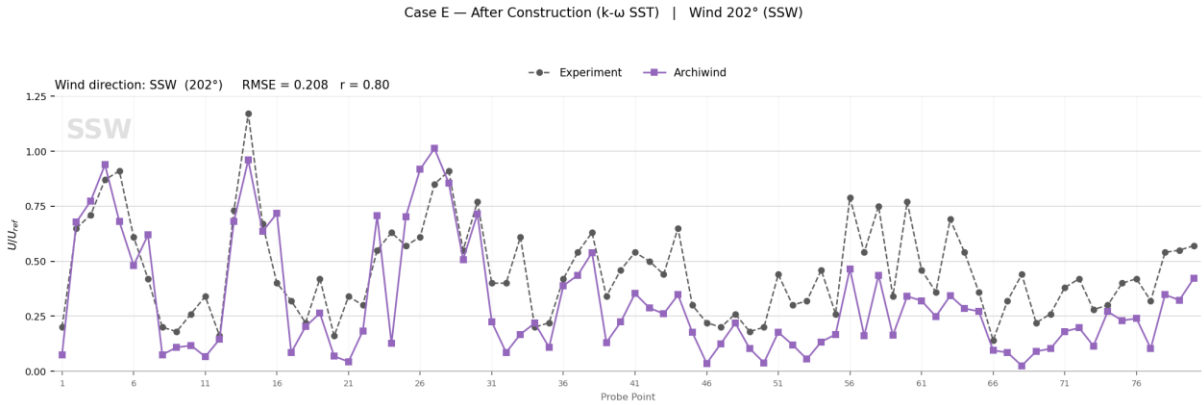
After Construction (k-ω SST) — Wind 135° (SE). RMSE = 0.150 r = 0.828



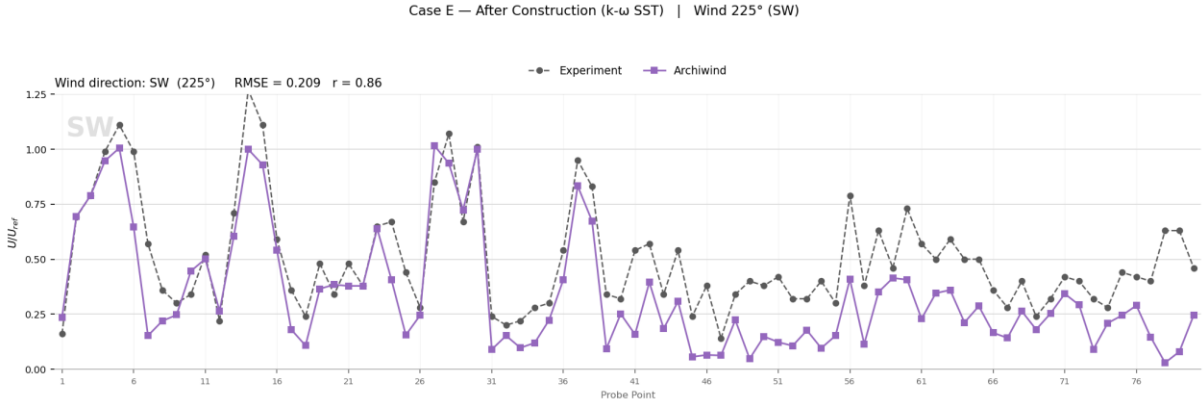
After Construction (k-ω SST) — Wind 157° (SSE). RMSE = 0.138 r = 0.783



After Construction (k-ω SST) — Wind 180° (S). RMSE = 0.165 r = 0.835



After Construction (k-ω SST) — Wind 202° (SSW). RMSE = 0.208 r = 0.800



After Construction (k-ω SST) — Wind 225° (SW). RMSE = 0.209 r = 0.860



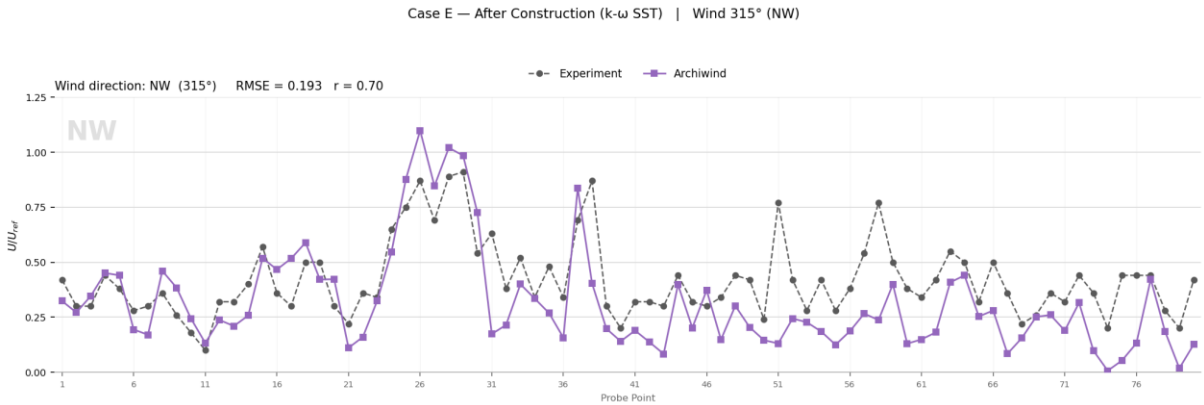
After Construction (k-ω SST) — Wind 247° (WSW). RMSE = 0.198 r = 0.801



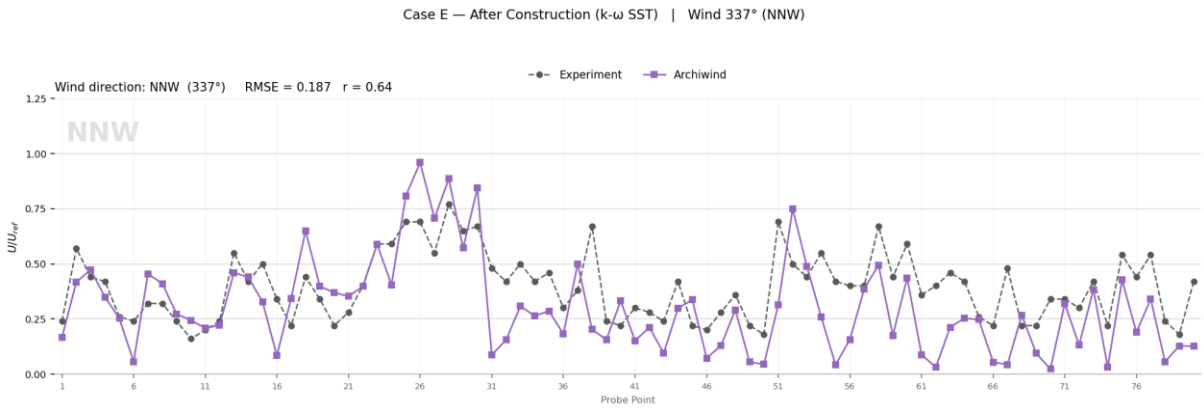
After Construction (k-ω SST) — Wind 270° (W). RMSE = 0.171 r = 0.830



After Construction (k-ω SST) — Wind 292° (WNW). RMSE = 0.180 r = 0.775



After Construction (k-ω SST) — Wind 315° (NW). RMSE = 0.193 r = 0.696



After Construction (k-ω SST) — Wind 337° (NNW). RMSE = 0.187 r = 0.636

REFERENCES

[1] Yoshie, R., Mochida, A., Tominaga, Y., Kataoka, H., Harimoto, K., Nozu, T., & Shirasawa, T. (2007). Cooperative project for CFD prediction of pedestrian wind environment in the Architectural Institute of Japan. Journal of Wind Engineering and Industrial Aerodynamics, 95(9–11), 1551–1578.

[2] Tominaga, Y., Mochida, A., Yoshie, R., Kataoka, H., Nozu, T., Yoshikawa, M., & Shirasawa, T. (2008). AIJ guidelines for practical applications of CFD to pedestrian wind environment around buildings. Journal of Wind Engineering and Industrial Aerodynamics, 96(10–11), 1749–1761.

[3] Shih, T.-H., Liou, W. W., Shabbir, A., Yang, Z., & Zhu, J. (1995). A new k-ε eddy-viscosity model for high Reynolds number turbulent flows. Computers & Fluids, 24(3), 227–238.

[4] Menter, F. R. (1994). Two-equation eddy-viscosity turbulence models for engineering applications. AIAA Journal, 32(8), 1598–1605.

[5] Franke, J., Hellsten, A., Schlünzen, H., & Carissimo, B. (2007). Best practice guideline for the CFD simulation of flows in the urban environment. COST Action 732, COST Office, Brussels.

[6] Blocken, B. (2015). Computational Fluid Dynamics for urban physics: Importance, scales, possibilities, limitations and ten tips and tricks towards accurate and reliable simulations. Building and Environment, 91, 219–245.

[7] Hågbo, T.-O., & Giljarhus, K. E. T. (2022). Pedestrian Wind Comfort Assessment Using Computational Fluid Dynamics Simulations With Varying Number of Wind Directions. Frontiers in Built Environment, 8, 858067. https://doi.org/10.3389/fbuil.2022.858067

[8] Taylor, P. A., & Teunissen, H. W. (1987). The Askervein Hill project: overview and background data. *Boundary-layer meteorology*, *39*(1), 15-39.

[9] Berg, J., Mann, J., Bechmann, A., Courtney, M. S., & Jørgensen, H. E. (2011). The Bolund experiment, part I: flow over a steep, three-dimensional hill. *Boundary-layer meteorology*, *141*(2), 219-243.